Intra-continental wildfire smoke transport and impact on local air quality observed by ground-based and satellite remote sensing in New York City

Yonghua Wu [1], Anny Arapi [1], Jianping Huang [2], Barry Gross [1], Fred Moshary [1]

[1] NOAA-CREST at the City College of New York (CCNY), New York, NY 10031, USA

[2] NOAA-NCEP Environmental Modeling Center (EMC) and IM System Group Inc., College Park, MD 20740, USA

Abstract The wildfires in Fort McMurray of Alberta, Canada, injected large amounts of smoke aerosols in May 2016 and were identified as being one of Canada's major weather events of the year. This paper presents a synergistic remote sensing and in-situ measurement of the resultant smoke plume transport, optical properties, and its impacts on local air quality in New York City (NYC). Comparisons with the operational air quality model forecast (the NOAA National Air Quality Forecasting Capability, NAQFC) performance are presented. The aloft plume intrusions on May 9-13 and 25-29, 2016, and their mixing down into the planetary-boundary layer (PBL) were observed by a combined lidar, ceilometer and other measurement. A decrease in single-scattering albedo and absorption Angstrom exponent near one indicates that the plumes were absorbing aerosol dominated. Dramatic impacts of smoke transport on the ground air quality are demonstrated with a coincident increase of ground $PM_{2.5}$ (from 5- to 25~30 $\mu g/m^3$) in NYC urban and upwind rural area, enhancement of the $PM_{2.5}$ speciation (organic carbon, elemental carbon, potassium ion (K^+)) and the ozone exceedance of NAAQS. Using the satellite and model product, we show regional spatial distribution of smoke, multiple transport paths and wildfire sources. Finally, with the lidar vertical profiling observations, we evaluate the model PBL-height (PBLH) and $PM_{2.5}$ during May 24th to 30th, 2016. The model PBLH shows consistent diurnal variation with the observed mixing layer height (MLH), but is clearly overestimated during the convective daytime hours. On the other hand, when estimating the MLH directly from the model $PM_{2.5}$ profile, better agreement with observation was indicated. This helps explain the good agreement between the model $PM_{2.5}$ and surface measurements except for the model overestimate during the morning of May 25 and 26, 2016.

Key words: Wildfire smoke, transport, air quality, lidar, model

1. Introduction

Wild fires emit large amounts of aerosols or particulates including black carbon (BC) and organic carbon (OC), as well as trace gases such as carbon monoxide (CO), carbon dioxide (CO_2), nitrogen oxides (NOx), volatile organic compounds (VOCs), etc. (Liu et al., 2014). Critical for health concerns, smoke particulates can be extremely small and result in increased health risk when mixed down into the surface layer. National ambient air quality standards (NAAQS) for fine particulates limit exposure to $PM_{2.5}$ (particle diameters <2.5 μm) to 24-hr average 35 $\mu g/m^3$ set by US Environmental Protection Agency (EPA) (Dawson et al., 2014). Wildfire emissions and associated ozone (O_3) precursors may result in exceedance of O_3 and/or $PM_{2.5}$ that is referred to the exceptional event in regulatory decisions regarding the NAAQS (Jaffe et al., 2013; Dreessen et al., 2016; Sapkota et al., 2005; Sofowote et al., 2015).

The frequency and intensity of wildfire events is expected to increase with climate change (Dennison et al., 2014; Schoennagel et al., 2017). Due to the need to forecast such events and issue warnings to vulnerable populations in urban areas, accurate Chemical Transport Models (CTM) that can quantify the effect of these events and follow the transport and chemical transformations to the surface level are needed. Unfortunately, the limitations of these models as well as difficulties in identifying and quantifying emission from fires make predictions very challenging. Adding to the difficulty is the nature of the urban environment where a complex urban surface is hard to parameterize in forecast models. For these reasons, model performance over urban areas have significant issues. For example, Hogrefe et al (2007) show that total $PM_{2.5}$ mass was strongly overestimated in the NYC metropolitan area; the analysis of species observations and model predictions shows that most of this over-prediction stems from organic aerosols and crustal material. A later study by Doraiswamy et al. (2010) demonstrates that the CMAQ model significantly over-predicts $PM_{2.5}$ in NYC during the summer both in the pre-morning and post-sunset hours. In trying to determine the root cause of these overestimations during specific periods, the need for vertical profiling studies becomes clear. In addressing these issues more directly, Zhang et al. (2012) indicate that the parameterizations for urban sublayer process and physiographic data are challenging but critically important for the $PM_{2.5}$ forecast in the urban areas since they effect pollutant turbulent mixing, dispersion and deposition. On the other hand, Gan et al (2011) use vertical profiling data from a ceilometer to explore the mass concentration over different vertical ranges and show that the integrated $PM_{2.5}$ mass diurnal pattern by the model was in agreement with the ceilometer observation. Further, it was shown that the periods of highest $PM_{2.5}$ over-biases in the model were due to under-predictions of the PBL height which itself was a consequence of incomplete modeling of urban heating processes in the PBL.

In addition, smoke from wildfires or biomass burning is one of the major sources in uncertainty of air quality model forecast. Smoke is a critical air pollutant subject to the NAAQS (Zhang et al., 2008; Huang et al., 2017; Miller, 2011). Many efforts have been made to improve modeling the impacts of wildfire emissions on air quality. National Air Quality Forecasting Capability (NAQFC) is a joint NOAA-NCEP regional operational weather forecasting model and EPA-CMAQ model (Lee et al., 2016; Huang et al., 2017). A major feature is the incorporation of real-time intermittent sources for particles emitted from wildfires within the NAQFC domain and windblown dust from outside the CMAQ by coupling to the NEMS global aerosol capability (NGAC) model, as well as a further upgrade for emission sources using the U.S. EPA's 2011 National Emission Inventory (NEI). Ingesting wildfire sources in particular are from satellite retrievals of fires sources and the estimation of the biomass emission footprints (Lee et al., 2016).

While urban local sources can lead to high $PM_{2.5}$ levels, the impact of continental transported plumes on $PM_{2.5}$ under conditions when smoke plumes advect into the PBL is not well understood. To explore this in more details, we study intense wildfire that began on May 1, 2016 in Fort McMurray, Alberta, Canada, forcing the largest wildfire evacuation in the province's history. The wildfire spread across approximately 590,000 hectares in northern Alberta and into Saskatchewan before it was declared to be under control on July 5, 2016. Such wildfires are mainly due to the dry and warm weather in spring. The smoke from these fires travelled across the U.S. to the Gulf coast and even to Europe according to multiple satellite images (https://en.wikipedia.org/wiki/Fort_McMurray).

While efforts have been made to use direct aerosol observations from satellites to estimate surface level $PM_{2.5}$ (Hoff et al., 2009), these studies assume the surface $PM_{2.5}$ is due to convective mixing of aerosols within the PBL. However, it is clear that aloft aerosol plumes (above the PBL) that can contribute to column total aerosol optical depth (AOD) have little connection with ground $PM_{2.5}$ (Engel-Cox et al., 2006; Han et al., 2015). Thus, vertical distributions and spatiotemporal variations of aerosols are critical to satellite remote sensing of ground $PM_{2.5}$ (Liu et al., 2011; Li et al., 2016; Zhang et al., 2015).

In this study, a synergistic remote sensing of wildfires smoke transport, sources, optical characteristics and impacts on the local air quality in New York City is presented by using a ground-based multi-wavelength elastic-Raman lidar, a ceilometer, a sun/sky radiometer, in-situ, satellite and model product in May 2016. The time-height distributions and optical properties of aerosols are presented to identify the intrusions of aerosol plumes and the mixing down of particulates in the PBL. The temporal variations of ground $PM_{2.5}$ and its main speciation (OC, EC, K^+, sulfate and nitrate, etc.) in the urban and upwind rural areas are analyzed to assess the smoke effects. Different transport paths and origins of smoke are investigated with the NOAA-HMS (hazard mapping system) product and HYSPLIT (Hybrid Single Particle Lagrangian Integrated Trajectory) back-trajectory analysis. Regional-scale spatial distribution of smoke plumes in the eastern US are shown from the satellite CALIPSO lidar. Using the remote sensing and in-situ observations, we evaluate the NAQFC product of $PM_{2.5}$ and PBLH. This paper is organized as follows. In Section 2, the observation instruments and the retrieval method of aerosol optical properties are discussed. In Section 3, the results and discussions on the transported smoke aerosols, as well as the variations of ground $PM_{2.5}$ and species are presented. Finally, Section 4 outlines the study's conclusions.

2. Methodology and Observations

2.1 Ground-based observations

A suite of ground-based remote sensing instruments were deployed for atmospheric observations at CCNY (40.821° N, 73.95° W), including a 3-wavelength Elastic-Raman lidar, a ceilometer (Vaisala CL-51), an AERONET Cimel sun/sky radiometer, a multi-filter shadow band radiometer (MFR-7) and a microwave radiometer (Radiometrics MP-3000A). Meanwhile, a standard surface air quality monitoring station is operated on the City College campus in NYC by the New York State Department of Environment Conservation (NYSDEC) making hourly $PM_{2.5}$, O_3 and CO measurements. Downwind of CCNY site (54 km northeast), there is another AERONET-site (LISCO, 40.955º N, 73.3419º W) and a national meteorological station at Upton New York (OKX, 40.87º N, 72.86º W) together with routine radiosonde launch for meteorological profiling observation.

The multi-wavelength Elastic-Raman lidar emits three wavelengths (355-, 532- and 1064-nm) at a repetition rate of 30 Hz (Spectra-physics Quanta-Ray PRO-320) (Wu et al., 2009). A receiver telescope (Ø50-cm) collects three elastic scattering and two Raman-scattering returns by nitrogen (N_2) and water vapor molecules excited by 355-nm laser output. The signals are acquired by a LICEL transient recorder (TR40-160) and recorded with 1-min average and 3.75-m range resolution. The signal at 1064-nm is highly sensitive to the aloft and thin aerosol layer since the molecular backscatter at this wavelength is much weaker than the aerosol. N_2-Raman returns can be used to derive aerosol extinction coefficients at 355-nm without an assumption of a lidar ratio constant but suffer from small signal-to-noise ratio (SNR) in the daytime. The elastic scattering signals are usually used for the daytime measurements (Fernald, 1984); and we use sunphotometer-measured aerosol optical depth (SP-AOD) to constrain the lidar-derived aerosol extinction profile or lidar-ratio. The lidar signals below 0.5-km altitude need to be corrected with the overlap function because of incomplete overlap between the transmitting beams and receiver's field-of-view. The lidar aerosol products include - aloft aerosol layer and cloud height, aerosol extinction coefficient and extinction-related Angstrom exponent (Gan et al., 2011; Wu et al., 2012). Generally, fine particulates such as smoke aerosols have relatively larger Angstrom exponent than the large coarse particles such as dust and sea salt (Eck et al., 1999). Due to eye safety limitations and the need for human observers, the system is usually operated for 2 to 3 days per week and mostly in the daytime on weekdays except for specific events where more extensive time observations are made. To help address this observational limitation, we also deploy a ceilometer (Vaisala CL-51) which measures laser backscatter at a wavelength of 910 nm as a function of height with a range resolution of 10 m (Münkel, 2004). It employs a pulsed InGaAs diode laser as the transmitter that emits eye-safe laser pulses (3 μJ/pulse) at high repetition rate (6.5 kHz). A single lens telescope is used for laser transmission and as the lidar receiver (Diameter=14.8 cm, F#3.0). The total attenuated backscatter or calibrated range-corrected backscatter coefficient is produced, which provides a possibility for studying dynamic PBL processes and evolution that can benefit long-term air pollution studies. Lower power allows for eye safety so that the CL-51 is fully automatic providing 24-hr/7-day operation in all-weather condition.

Planetary boundary layer (PBL) is the lowest level of the atmosphere where is directly and strongly influenced by the underlying surface (Stull, 1988). The PBL-height (PBLH) is a key parameter in the air quality and weather modeling. The mixing-layer height (MLH) is the height up to which atmospheric properties or substances (e.g. aerosols and water vapor) originating from the Earth's surface or formed within this layer are dispersed almost uniformly over the entire depth of this layer by turbulent vertical mixing processes. According to Stull (1988), a convective boundary layer (CBL) that occurs during the daytime is usually referred as a mixing layer. At top of CBL, there is an entrainment zone (EZ) where air aloft is entrained and mixed into the aerosol-laden and moister PBL. The lidar-measured MLH in the daytime represents the convective PBLH (Cohn et al., 2000; Menut et al., 1999), usually taking as the middle of EZ. In this study, a wavelet transform technique is used to estimate the MLH where the lidar or ceilometer backscatter profile often shows the largest gradient associated with the aerosol loadings (Gan et al., 2011).

In addition, AERONET sun/sky radiometer provides direct measurements of column AOD and Angstrom exponent (AE), and can retrieve relevant aerosol microphysical parameters such as volume size distribution, refractive index and single scattering albedo (SSA) through multi-angle sky radiance measurements (Holben et al., 1998; Duboviok et al., 2000). Absorption AOD and its spectral dependence (i.e. Absorption Angstrom exponent or AAE) can be also derived. For "pure" BC in the atmosphere, the AAE is assumed to be one (Bond and Bergstrom, 2006) and observations of AAE greater than one are often taken as evidence of brown carbon (BrC) or dust (Russell et al., 2010). Typically, the uncertainty in AERONET-sun photometer AOD under cloud-free conditions is within ±0.01 for λ>440 nm and less than

±0.02 for shorter wavelengths (Hoblen et al., 1998; Eck et al., 1999). Error for particle size distribution is estimated to be 15~25% of the radius between 0.1 and 7 μm (Dubrovnik et al., 2000). In this study, Level-1.5 cloud-screen product of AOD and AE are used (http://aeronet.gsfc.nasa.gov/). The data at the LISCO-site (a downwind area near the lidar site) are used since the instrument at CCNY site was taken down for the calibration during the period of this study.

Additionally, New York State Department of Environment Conservation (NYSDEC) samples $PM_{2.5}$ and PM speciation (OC, EC, Sulfate, etc.) in both urban and non-urban sites (Rattigan et al., 2010, 2016). At CCNY campus, there is an air quality-monitoring site where the $PM_{2.5}$, O_3 and CO are reported hourly. The $PM_{2.5}$ and its speciation are routinely monitored at Queens College site (QC, 40.736º N/73.822º W, 14 km southeast from CCNY as shown in Fig.1a below) in NYC. The Newburgh site (41.499 º N/74.01 º W) located in the north of CCNY (~76 km away) is herein referred to a non-urban or rural site, and the data are useful for evaluating the transport effect. On the other hand, the site of Division Street is located in southern Manhattan, NYC. The hourly OC, EC and sulfate of $PM_{2.5}$ are measured using the Sunset OC/EC field analyzer (Sunset Lab, Inc.) and sulfate particulate analyzer (SPA, Thermo Electron Company, model 5020), respectively. In addition, the daily average $PM_{2.5}$ species are measured using integrated filter-based method once-every-3-day (1-in-3 day) following the planned schedule in the EPA's Chemical Speciation Network (CSN) (Oliver et al., 2010). Measurement errors of $PM_{2.5}$ include uncertainty in cut point tolerances, particle bounce and re-entrainment, impaction surface overloading, and losses to sampler internal surfaces. Relative uncertainty is generally ±15% for Federal Reference Method (FRM) $PM_{2.5}$ mass measurement based on the previous studies (Rees et al., 2004; Hains et al., 2007).

2.2 Satellite products

The NOAA Hazard Mapping System (HMS) was developed in 2001 by the National Environmental Satellite and Data Information Service (NESDIS) as an interactive tool to identify fires and the smoke emissions over North America in an operational environment. The system utilizes two geostationary and five polar orbiting environmental satellites (Ruminski et al., 2016). The result is a quality-controlled display of the locations of fires and significant smoke plumes. HMS has a number of detection limitations such as clouds hindering detections, no vertical structure information and no quantitative amount or density of smokes and only available during daylight. In addition, the NOAA-HYSPLIT model is used to compute air parcel trajectories and model the dispersion and the route of airborne particles (Draxler et al., 1997) and can be used either in a back-trajectory mode to analyze sources or in forecast mode.

CALIOP (Cloud-Aerosol Lidar with Orthogonal Polarization) instrument, on board the CALIPSO satellite platform, is a spaceborne polarization-sensitive two-wavelength (532- and 1064-nm) lidar (Winker et al., 2009). It observes global aerosol/cloud vertical distribution and provides aerosol type classification and optical properties products. CALIPSO has a narrow laser footprint (~70 m) at the earth's surface and a 16-day revisit cycle. The laser pulse repetition frequency of 20.16 Hz produces profile every 335 m along the ground. In this study, the latest release product (Version 4.10, Level-1 attenuated backscatters, linear volume depolarization ratio and Level-2 aerosol extinction and aerosol type classification) are used.

2.3 NAQFC (the NOAA National Air Quality Forecasting Capability) model

NAQFC consists of the NOAA-NCEP regional operational weather forecasting model (NAM-North America Model) and EPA-CMAQ model (Lee et al., 2016; Huang et al., 2017). It is designed to provide 2-day model forecasts of O_3 and fine particulates ($PM_{2.5}$) twice per day at the 06 and 12 UTC cycles. For the study, products with spatial resolution of 12 km at the 06 UTC are used. The NAQFC program performs incremental tests and evaluations verified against the U.S. EPA AIRNow surface monitoring network.

A modified version of the U. S. EPA CMAQ model (version 4.6) dubbed CMAQ v4.6.5, is run with 12 km horizontal grid spacing with a Lambert Conformal Conic (LCC) map projection for the product used in this study. The offline coupling between NWS/NCEP NAM meteorological model and CMAQ is achieved by two pre-processors. In addition to the coupled NMMB-CMAQ system, there are other components such as the emission module and the chemical lateral boundary condition builder as well as the product generating post-processing components. Emission inventories are processed by sectors, but the fire sectors do not include prescribed burns and wildfires from the National Emission Inventory (NEI). The U.S.

EPA-NEI 2011 version-1 is being incorporated into Premaq's emission projection schemes. The 2006 Environment Canada National Inventory sources were used for Canada, and the 2012 Mexico NEI non-road sources were used for Mexico. The emissions from wildfires, prescribed agricultural burns, and land clearing fires were computed using the dynamic fire emission modeling U.S. Forest Service BlueSky smoke emission package (O'Neill et al., 2009) and the NOAA-HMS for fire locations and strength. Wildfires that are estimated to last at least 24 hours are used as emission sources into the NAQFC.

The NAQFC CMAQv4.6.5 follows largely the U.S. EPA Aero4 module and the related emission and removal processes found in the U.S. EPA-CMAQ version 4.6 (Foley et al., 2010). Gas to particle conversion, heterogeneous reactions, depositional growth, and coagulation are included (Kelly et al., 2009). The Aero4 module simulates particle formation, condensational and coagulation growth or evaporative dissipation of existing particles due to ambient chemical, temperature and humidity conditions. The detailed configuration for NAM-CMAQ system can be found in Lee et al. (2016). The Mellor Yamada Janjic (MYJ) PBL scheme (Janjie et al., 2001) is used in this version of NAM.

3. Results and discussions

3.1 Temporal variation of $PM_{2.5}$

Figure 1 shows the geolocation of $PM_{2.5}$ sites and temporal variation of ground $PM_{2.5}$ in the urban and non-urban areas of NYC in May 2016. As shown in Fig.1 (a), Newburgh-site represents a non-urban site to the north of the CCNY-site while other sites are located in the NYC urban area. The average $PM_{2.5}$ over the 15 urban sites are also given. It can be seen that there are two significant elevated $PM_{2.5}$ events (episode-1 on May 9-13 and episode-2 on May 25-29). The comparison of $PM_{2.5}$ among the urban and non-urban sites for these two cases shows the strong regional footprint of the enhanced $PM_{2.5}$, indicating that this is not due to local sources but is likely due to transported sources into the NYC area. The dramatic nature of these events can be seen by the large increase in $PM_{2.5}$ from the background levels. For example, at the CCNY site, the $PM_{2.5}$ concentrations increased from 5- to 30-$\mu g/m^3$ on May 25-27.

Figure 2 gives the temporal variation of the $PM_{2.5}$ speciation and O_3 at Queens-College (QC) site. In Fig.2 (a), both the OC and EC show consistent increase with a dominant OC concentration for the two episodes. For instance, the hourly OC increases from 2 μg/m^3 to 8 μg/m^3 while the hourly EC increases up to 4 μg/m^3 during May 25-27. Meanwhile, the sulfate also indicates a clear increasing trend from May 25 to 27. These values are much larger than the monthly average of OC (1.0~ 4 μg/m^3), EC (0.5~1.4 μg/m^3) and sulfate (1~3 μg/m^3) in NYC based on the multi-year data (Rattigan et al., 2010, 2016; Masiol et al., 2017). Importantly, the O_3 concentrations were in exceedance of NAAQS (70-ppb) for the episode-2 on May 25-26. The daily average of $PM_{2.5}$ species from Chemical Speciation Network monitors (1-in-3 day) at Queens College are given in Fig.2 (c), which indicate consistently high OC on May 9 and 27, respectively. In addition, Potassium ion (K^+) acts as a useful tracer of wildfire smoke because there are few anthropogenic sources, and its concentrations above background levels are a signature of wildfire emissions (Pachon et al., 2013; Dreessen et al., 2016). As shown in Fig.2 (d), the K^+ concentrations are amplified in the period of episode-I and II. Daily average concentration of K^+ on May 9-12 (20-22 ng/m^3) and May 24-27 (26-42 ng/m^3) are much bigger than the value (2.7-6.0 ng/m^3) on the other days in the same month. These results indicate the smoke-dominated plume transport and possible mixture with the upwind industrial aerosols (i.e. sulfate) along the transport path.

The correlation between the $PM_{2.5}$ concentrations at the CCNY (urban) and Newburgh (rural) is very high with a correlation coefficient (R~0.84) and the linear regressions slope of 0.94 (see Fig.3). In addition, the $PM_{2.5}$ at the upwind rural sites of Whiteface and Pinnacle (atmosphere background site operated by NYSDEC) also shows similar trends to the data at CCNY. Thus, such coincident increase and good correlation are good indicators that the $PM_{2.5}$ at those sites are probably from the similar sources that is associated with the long-range transport of smoke.

3.2 Time-height distribution and optical properties of aerosols

3.2.1 Episode-1 on May 9-13

The time-height distributions of aerosols and clouds are shown in Fig. 4 from the lidar-ceilometer measured attenuated backscatter during May 9-13, 2016. Some clouds are labeled (dark-red in color) by showing much stronger backscatter signals than the aerosols but much weaker signals above the cloud due to strong attenuation of cloud. As shown in Fig. 4(a), the lidar data in the daytime of May 9-12 shows deep mixing-layer height (MLH) at ~2.5 km on May 9, and the stratification structures or multiple layers of aerosols can be clearly seen in the free troposphere on May 10-12. The MLHs are generally lower than 1.5 km on May 11-12. As shown in Fig.4 (b) from the ceilometer measurement, in the early morning of May 9, an aloft layer of aerosols showed a gradual subsidence and then mixed down into PBL at 6 am. A regional sinking air in the northeast coast of US was indicated from the NOAA/NCEP vertical wind velocity at the 850-mbar level at 6:00 UTC on May 9, 2016 (see Fig.10 (d)), which in combination with strongly convective PBL provides a favorable condition for the plume mixed and transported to the ground. These dense aloft aerosols are likely from the long-range transport of plumes due to their isolation from the local near-surface emissions or pollutants. Meanwhile, the mixing and dispersion of aerosol plumes in the PBL was expected in the convective PBL during solar heating of the atmosphere after sunrise. Figure 4(c) shows the continuous 24-hr measurements during May 8-13. Some rainfall occurred in the morning of May 8 and then followed with the clean sky. During May 11 and 12, other aloft aerosol layers were persistently observed around 2-km; and strong backscatters in the PBL indicate generally larger aerosol concentrations.

The aerosol extinction coefficients and AOD are derived from the CCNY-lidar and shown in Fig. 5. On May 9 in Fig.5 (a), the peak extinction of aerosols attains 0.1 km^{-1} at 532-nm, and the aloft aerosol layers generally show the extinction coefficient less than 0.05 km^{-1}. The extinction-related Angstrom exponents are estimated in range of 1.5 to 2.5 on May 9-12, which imply the fine-mode dominated aerosols. Figure 5(b) gives the aloft-layer fraction in the total AOD. The aloft-layer-fraction in the total AOD is generally lower than 0.2 on May 9 but becomes larger on May 11-12 with the value of 0.4-0.6. Such AOD contribution by the aloft-layer may cause major difficulties in using satellite-measured column AOD to estimate ground PM$_{2.5}$.

3.2.2 Episode-2 on May 25-29

Figure 6 shows the time-height distributions of aerosols during May 24-29, 2016. In Fig.6 (a), the lidar measurements indicate the deep mixing-layer-heights (dash line in the figure) over the convective daytime period on May 25, and the aloft aerosols are clearly visible above the PBL on May 26 and 27. As shown in Fig.6 (b) from the ceilometer measurement, starting from 5:00 am on May 25, two aloft aerosols layers appeared in the PBL, one below 1-km and other at 2~3 km at noon. In particular, the PBL heights show a dramatic increase and reaches up to 3 km in the afternoon, which indicate strong convective or turbulent process resulting in plume mixing within the PBL. Figure 6(c) shows the 24-hr measurements during May 24-29. Some rainfall occurred in the morning of May 24. During May 25-28, the PBL-tops show strong diurnal variation with the maximum height of 2.5~3 km at midday but below 1-km at night. Some aloft aerosol layers are indicated in the morning of May 27, and then descend to the surface in the afternoon and night of May 27. Finally, on May 29, the PBL heights become lower at 1.5 km with the smaller attenuated backscatters, and later some rainfall occurs by mid-night.

The aerosol extinction coefficients are derived from the CCNY-lidar and shown in Fig. 7. In Fig.7 (a) on May 25, the peak extinction of aerosols attains 0.2 km^{-1} at 532-nm with the Angstrom exponents of 1.5~1.7 in Fig.7 (b) that indicate fine-mode particles dominated. The dense aerosol layers at 1.0-2.5 km can be clearly seen before 14:00. Meanwhile, Figure 7(b) shows the profiles of aerosol extinction coefficients at thee-wavelength and Angstrom exponents over half-hour average. They show similar structure of aerosols; and the good consistency of 355-nm extinctions between the two independent retrievals from the Raman- and elastic-scattering signals verifies the reliability of retrievals. In addition, the lidar-derived aerosol optical depths vary from 0.2 to 0.4 at 532-nm that indicate more aerosol loading than the one in episode-I. On May 26, the aerosol extinction coefficients in the PBL are in the range of 0.05 – 0.2 km^{-1} while the PBL-tops reach 2.5 km at 11:00 am-6:00 pm. On May 27, more aloft plumes can be seen below 4-km while the MLHs are around 2-km altitude. In addition, the mean of the Raman-lidar derived lidar-ratio in the PBL was found to be around 61.4 +/- 5.9 sr at 355-nm that denotes smoke-like particles (Omar et al., 2009).

The correlation between the ground $PM_{2.5}$ and ceilometer-measured attenuated backscatter at near surface is analyzed, and the results in Fig. 8 indicate the modestly high correlation coefficient of 0.7. The relative humidity is generally lower than 70% that means that the moisture is not playing a major role in enhancing the aerosol backscatter. Thus, the ceilometer-measured attenuated backscatter can serve as a reasonable proxy for $PM_{2.5}$ comparisons with models.

Figure 9 shows the column aerosol optical properties from the AERONET-measurements. A consistent increase of AOD from 0.18 to 0.45 at 532-nm can be seen on May 25 while the Angstrom exponents are in range of 1.6 - 1.4 at the wavelength pair of 440-870-nm. The single scattering albedos in Fig.9 (b) decreases from the morning to the afternoon (15:52 local time or eastern daylight saving time). We calculate the absorption Angstrom exponents (AAE) at 440-870 nm; it shows a decrease from 1.4 to 1.08 along the plume intrusion. The AAE value with the aerosol plume is close to the vaue of 1.0 for black carbon (Russell et al., 2010). These results suggest the increase in absorbing particles due to intrusion of transported smoke on May 25. On May 26, the AODs are in the range of 0.25 - 0.45 while the extinction-related Angstrom exponent are smaller than 1.6. On May 27-28, the Angstrom exponents become relatively higher (1.6 - 1.8) but then decrease (1.2-1.6) on May 29. Such temporal variation of Angstrom exponents might correspond to different types of aerosols associated with the transport and mixture with local aerosols.

3.3 Source and transport path of wildfire smoke

Figure 10 shows the MODIS RGB image that indicates the wildfires and smoke over southwestern Canada (Alberta, Saskatchewan, and Manitoba) and northern boundary of U.S on May 8 (Episode-1). The wildfire points and smoke dispersion areas are shown in Fig.10 (b) from the NOAA-HMS product, where the red symbol ‘x’ represents the fire burning points and the yellow areas denote the smoke dispersion/diffusion region. The results indicate the wildfires at Fort McMurray of Alberta spreading into Saskatchewan and U.S. The numerous severe wildfires burned around Fort McMurray, Alberta, Canada since May 4. In addition, Fig.10 (b) shows the air backward trajectories with the end points at CCNY-lidar site (6:00 UTC on May 9, 72-hr long at the altitude of 1-km and 2-km). The results verify that the air parcels in the PBL in

NYC are transported from the wildfire regions in Canada and northwest U.S. Figure 10 (c) shows the surface smoke content from the NAAPS (Navy Aerosol Analysis and Prediction System) model and air backward trajectories at 1-2 km on May 9. The results indicate the relatively high concentration of smoke along the transport path from the northwest US and Canada to NYC.

Figure 11 gives the wildfires and smoke sources on May 25-27 (Episode-2), as well as the backward trajectories with the end points at the sites of CCNY, QC and Newburgh (12:00 UTC, 72-hr long, at the altitude of 0.5-km, 1-km and 2-km), respectively. Interestingly, similar trajectories of transport are indicated among the three sites and at the different altitudes. However, the transport paths show significant shift during May 25-27, from western Canada to western and southeast US. There are still numerous wildfires at Fort McMurray, Alberta, Canada and some wildfires from Mexican, Central American and Arizona. Please note that the extensive cloud cover hinders the smoke detection by satellites on these days that are clearly shown on the satellite visible images. It can be seen in Fig.11 that the smoke over NYC on May 25 was transported from Canada. On May 26-27 in Fig.11 (b-c), the air was transported from the western and southeast US where there are the smoke originated from Canada.

3.4 Regional aerosol distribution in the northeast U.S.

Spatial and range-solved distribution of aerosols are shown in Fig. 12 from the satellite NOAA-GOES and NASA-CALIPSO measurements on May 12, 2016. Figure 12 (a) displays the relatively high AOD in the northeast US that are associated with the smoke transport, but there are many clouds in the North US and Southern Canada, which prevent the smoke detection from the satellite measurement. The CALIPSO data in Fig.12 (b) show that the aloft plumes are located below 5-km in the latitude of 41°N ~ 50°N in the early morning of May 12. The aerosol extinctions are in range of 0.05~0.2 km^{-1} at 532-nm in Fig. 12(c) and the elevated layers are mostly classified as smoke in Fig.12 (d).

Figure 13 shows the aerosol spatial distribution on May 26 in the eastern US. In this case, the aerosol layers are mostly located in the PBL (< 3-km) in the latitude of 30° N ~ 44° N. There are some low- and high-level clouds blocking the detection of aerosol layers as shown in Fig.13 (b). The aerosols in the PBL are partly classified as polluted continental/smoke or polluted dust nearby NYC (arrow position in the x-axis in Fig.13(c). This seems not consistent with the fact that the organic carbon are major components of $PM_{2.5}$ with less soil component in NYC (see Fig.2a and Fig.2c). The classification of polluted dust depends on an arbitrary threshold at 0.075 of depolarization ratio (Omar, et al., 2009); and the over-classification of polluted dust for the smoke-dominant events have been observed in the previous literatures (Burton et al., 2013; Wu et al., 2017). The average depolarization ratio in the PBL (<2.5 km) is mostly in the range of 0.05 to 0.09 at 30° ~ 45° N latitude, and 0.01 to 0.04 at 46° ~52° N latitude. The causes of depolarization by smoke are not well understood, which may be related to coated soot aggregates, lifting of surface soil into the smoke plume and asymmetry of smoke particles (Burton et al., 2015). As the same lidar-ratio (70-sr at 532-nm) is used in retrieving aerosol extinctions for the type of polluted continental and smoke aerosols, such misclassification of smoke as polluted continental aerosols will not affect the retrievals. Figure 3(d) show good consistency of the aerosol extinction coefficients between the ground lidar and CALIPSO product nearby CCNY-site.

3.5 Model $PM_{2.5}$ and PBL-height verification

Besides getting a better understanding of the properties of transported aerosol plumes with our vertical profiling instruments, a more direct assessment of the NAQFC product of PBL-height (PBLH) and ground $PM_{2.5}$ can be made with our measurements. Only the episode-II (May 25-29) is selected because the current NAQFC considers the wildfire emissions only over the continental US. To verify the reliability of ceilometer-observed PBLH, we firstly analyze the correlation between the ceilometer and lidar-measured convective PBLH; they show excellent linear correlation (Slope= 0.96 and correlation R= 0.81) as shown in Fig.14 (a) even to heights of 3 km. The comparisons of the PBLH between the model and ceilometer observations are shown in Fig.14 (b). Both show similar diurnal variation of PBLH, e.g. high PBLH at noon and afternoon but low PBLH at night. The model convective PBLH at noon are much higher than the observation. For instance, the model PBLH on May 25 attains 4.5 km while the measured PBLH is around 3.0 km. We further calculate the PBLH using the gradient variation of the model $PM_{2.5}$ mass vertical distributions with a wavelet transform technique (Gan et al., 2011). The results in Fig.14(c) indicate lower than the original or meteorological-based PBLH from the NAM model product in the daytime and are closer to the observation. Figure 14(d) shows the hourly $PM_{2.5}$ from the model and observation at CCNY-site. At first, the model product shows generally good agreement with the observations except some overestimation in the model during the morning of May 25 and 26. In fact, taken over the whole event, the model $PM_{2.5}$ shows similar temporal variation to measurements before (May 24) and after (May 29-30) the plume intrusion. Additionally, the comparison of model $PM_{2.5}$ at the other two sites (QC and IS-52) also indicate a similar consistency (not shown here).

As seen in Fig. 14(c) for the time-height distribution of $PM_{2.5}$ from the model, the aerosols show some elevated layers up to 4-km in the daytime of May 25 and 26, then become lower at 2-km on May 27-29, which is consistent with the lidar- ceilometer profiles in Fig.6. In particular, this shows the danger of using the meteorological-based PBL height output as the only indicator of vertical aerosol extent. Even the small overestimations of the $PM_{2.5}$ seem to be at least partially explained by the model placement of the $PM_{2.5}$ mass that is actually somewhat compressed by the low PBL.

3.6 Discussions

The wildfire smoke transport to NYC was proposed by a synergistic ground-based, satellite remote sensing and in-situ measurement in May 2016. In particular, continuous time-height distribution of aerosol measured by a lidar and ceilometer indicate the aloft smoke intrusion and mixing down into PBL. The mechanisms of plume mixing into PBL and ground depend on the synoptic weather process (e.g. air subsidence), plume height, PBL height and entrainment process. Our study indicates that regional air subsidence in the NE US, high PBLH (2.5~3.0 km) and PBL entrainment in the daytime provide favorable condition for plume vertical mixing down and transport to the ground. Colarco et al. (2004) simulated the mechanism of a Canadian Quebec wildfire plume aloft mixing down to the surface using a model on July 7, 2002 in Washington DC area of US. The results indicate that the PBL entrainment plays a major role while the subsidence alone was not enough to explain how the fire smoke was transported from an elevated layer to surface. However, large uncertainties in the model simulations are from the magnitude and injection altitude of fire emissions. On the other hand, Pahlow et al (2005) observed the smoke layer from Canadian Quebec wildfire descending to lower altitude in the PBL in the morning of July 6-8 2002 at Baltimore, MA (northeast US); and attributed this to the thermals overshooting at the PBL-top that coincide with upward and downward movements of air. In addition, Duck et al. (2007) showed that the arrival of biomass burning emissions at the surface from Alaska to the northeast coast of North America was associated with the synoptic-scale conditions (e.g. high-pressure ridge).

During the period of the two episodes, the coincident increase of ground $PM_{2.5}$ and its species (OC, EC, K^+) in the urban and rural area indicate the regional transport of the smoke. The OC/EC ratio has been used to confirm the profiles of biomass burning and mobile sources since biomass burning usually has higher OC/EC ratios (7-15) than gasoline (3.0-4.0) or diesel vehicles (<1.0) (Pachon et al., 2013). The OC/EC ratio in this study is in range of 3.0-8.0 for the episode I and II (not shown), which indicates the wildfires smoke. Importantly, the ozone concentrations are in the exceedance of NAAQS (O_3 >70 ppb) on May 25-26 that demonstrates the big impact of wildfire smoke on the local air quality. Thus, the episode-II may be referred to an exceptional event due to the wildfires smoke transport (Geigert et al., 2017). It is difficult to quantify wildfire smoke contribution to the ground $PM_{2.5}$ and O_3 concentrations, particularly when mixed with urban pollution and the secondary aerosol and ozone formed. It is challenging to separate the transported smoke from the local emission though the temporal variations of ground $PM_{2.5}$ before and after the plume intrusions can verify the smoke-associated enhancement of $PM_{2.5}$.

In addition, it is challenging to model $PM_{2.5}$ and PBLH in the complex urban environment. The comparisons of $PM_{2.5}$ and PBLH between the NAQFC product and our observations generally show consistent diurnal variation, but the meteorological-based PBLH from the model output is overestimated in the mid-day with a strong convection. When we calculate the PBLH using the model $PM_{2.5}$ vertical profile, the estimated PBLH agree well with the lidar observation. This implies that the meteorological-driven PBLH may not always represent the aerosol volumes in the atmosphere, which partly explain why the model $PM_{2.5}$ are over-predicted in the night. Dreessen et al (2017) show a case study on the Canadian wildfire smoke affected air quality in Maryland, US during June 9–12, 2015, which in particular resulted in a multiday O_3 exceedance of the NAAQS. The results indicate that CMAQ model under-predicted ozone formation by around 14 ppb in Maryland, and need adequate means to quantify and justify ozone impacts from wildfires.

4. Conclusion

This paper has analyzed the Canadian wildfire smoke transports that affect the local air quality in NYC in May 2016. The results demonstrate the intrusions of smoke plumes and mixing down into the PBL. The high MLH at 2.5~3 km and regional air subsidence imply favorable vertical transport and mixing condition. The elevated smoke contributes 40~60% fraction to the total column AOD based on the lidar profiling observation on May 12, which indicates the cautions to estimate ground $PM_{2.5}$ using the satellite-measured column AOD. The coincident increase and strong correlation of ground $PM_{2.5}$ in the urban and upwind rural areas indicate that the dominant mechanism is regional transport. The concurrent enhancement of OC, EC, K^+ and sulfate indicate the smoke transport and mixture with industrial emissions in the upwind area. The ground O_3 concentrations are in exceedance of NAAQS for the episode-II that may be referred as an exceptional pollution event. The severe wildfires and smoke sources in Fort McMurray, Alberta, Canada are verified to be the cause of episode-1 on May 9. The episode-2 on May 25-29 shows the daily variations of aerosol transport path and optical properties.

Our assessment of the NAQFC (NAM-CMAQ) indicate a similar diurnal variation of PBLH except an overestimate by the model in the convective daytime. We find that the PBLH estimated from the model $PM_{2.5}$ profiles agrees well with the observation in contrast to the model meteorologically derived PBLH. This demonstrates that the model derived PBLH is not always the best indicator of the vertical depth of the boundary layer aerosols. The model $PM_{2.5}$ agrees well with the observation during May 24-30 except for an overestimate by the model in the morning of May 25-26, which may be associated with the lower PBLH and vertical mixing of aerosol in the model.

Acknowledgements. This study is in part supported by the New York State Energy Resources Development Authority (grant # 100415), and The National Oceanic and Atmospheric Administration – Cooperative Science Center for Earth System Sciences and Remote Sensing Technologies (NOAA-CREST) under the Cooperative Agreement Grant # NA16SEC4810008. Authors greatly appreciate the data from NASA-AERONET, CALIPSO, NOAA-HMS, HYSPLIT model, and NYSDEC. In particular, we appreciate Oliver Rattigan for providing PM2.5 species data and reviewing this paper, Mike Ku and Winston Hao of NYSDEC for the discussions of model data. We are thankful to Jeff McQueen of NOAA/NWS/NCEP for providing the NAQFC product and reviewing the manuscript with great comments. We gratefully acknowledged the constructive comments from two anonymous reviewers that improve the manuscript.

References

Bond, T.C., R.W. Bergstrom, 2006. Light absorption by carbonaceous particles: an investigative review, Aerosol Sci. Tech., 40, 27–67.

Burton, S. P., R. A. Ferrare, M. A. Vaughan, A. H. Omar, R. R. Rogers, C. A. Hostetler, J. W. Hair, 2013. Aerosol classification from airborne HSRL and comparisons with the CALIPSO vertical feature mask, Atmos. Meas. Tech., 6, 1397–1412.

Burton, S. P., Hair, J. W., Kahnert, M., Ferrare, R. A., Hostetler, C. A., Cook, A. L., Harper, D. B., Berkoff, T. A., Seaman, S. T., Collins, J. E., Fenn, M. A., and Rogers, R. R., 2015. Observations of the spectral dependence of linear particle depolarization ratio of aerosols using NASA Langley airborne High Spectral Resolution Lidar, Atmos. Chem. Phys., 15, 13453-13473.

Cohn, SA, Angevine WM, 2000. Boundary Layer Height and Entrainment Zone Thickness Measured by Lidars and Wind Profiling Radars. J Appl. Meteorol. 39: 1233–1247.

Colarco, P. R., Schoeberl, M. R., Doddridge, et al. 2004. Transport of smoke from Canadian forest fire to the surface near Washington, D.C.: Injection height, entrainment, and optical properties. J.Geophy.Res., 109, D06203, doi:10.1029/2003JD004248.

Dawson, J. P., Bryan J. Bloomer, Darrell A. Winner, and Christopher P. Weaver, 2014. Understanding the Meteorological Drivers of U.S. Particulate Matter Concentrations in a Changing Climate. Bull. Amer. Meteor. Soc., **95**, 521–532.

Dennison, P. E., S. C. Brewer, J. D. Arnold, and M. A. Moritz, 2014. Large wildfire trends in the western United States, 1984–2011. *Geophys. Res. Lett.*, **41**, 2928–2933, doi: 10.1002/2014GL059576.

Doraiswamy, P., Hogrefe, C., Hao, W., Civerolo, K., Ku, J-Y., Sistla, G. A., 2010. Retrospective Comparison of Model-Based Forecasted PM2.5 Concentrations with Measurements, J. Air & Waste Management, **60** (11): 1293-1308.

Draxler, R.R., Hess, G.D., 1997. Description of the HYSPLIT_4 modeling system. NOAA Tech. Memo. ERL ARL-224, NOAA Air Resources Laboratory, Silver Spring, MD, 24.

Dreessen, J., Sullivan, J., Delgado, R., 2016. Observations and impacts of transported Canadian wildfire smoke on ozone and aerosol air quality in the Maryland region on June 9–12, 2015, J. Air & Waste Management Assoc., 66:9, 842-862, DOI: 10.1080/10962247.2016.1161674.

Dubovik, O., Smirnov, A., Holben, B. N., et al., 2000. Accuracy assessments of aerosol optical properties retrieved from AERONET Sun and sky radiance measurements. J. Geophys. Res., 105, 9791–9806.

Duck, T.J., Firanski, B. J., Millet, D.B., et al., 2007. Transport of forest fire emissions from Alaska and the Yukon Territory to Nova Scotia during summer 2004. J. Geophys. Res., 112, D10S44, doi:10.1029/2006JD007716.

Dutkiewicz, V. A., S. Qureshi, A.R. Khan, V. Ferraro, J. Schwab, K. Demerjian, L. Husain, 2004. Sources of fine particulate sulfate in New York, Atmos. Environ., 38(20), 3179-3189.

Eck, T. F., B. N. Holben, J. S. Reid, et al., 1999. Wavelength dependence of the optical depth of biomass burning, urban, and desert dust aerosols, J. Geophys. Res., 104, 31,333–31,349.

Engel-Cox, Hoff, R. M., et al., 2006. Integrating lidar and satellite optical depth with ambient monitoring for 3-dimensional particulate characterization. *Atmos. Environ.* 40, 8056– 8067.

Fernald, F. G., 1984. Analysis of atmospheric lidar observations: some comments. Appl. Opt. 23, 652-653.

Foley, K. M., Roselle, S. J., Appel, K. W., Bhave, P. V., Pleim, J. E., Otte, T. L., Mathur, R., Sarwar, G., Young, J. O., Gilliam, R. C., Nolte, C. G., Kelly, J. T., Gilliland, A. B., and Bash, J. O., 2010. Incremental testing of the Community Multiscale Air Quality (CMAQ) modeling system version 4.7, Geosci. Model Dev., 3, 205-226.

Fort McMurray wildfire on https://en.wikipedia.org/wiki/2016_Fort_McMurray_wildfire.

Gan, C., Wu, Y., Madhavan, B., Gross, B., Moshary, F., 2011. Application of active optical sensors to probe the vertical structure of the urban boundary layer and assess anomalies in air quality model PM2.5 forecasts, *Atmos. Environ.*, 45 (37), 6613-6621.

Geigert, M., May 2016 Ozone exceptional event analysis for Connecticut using satellite data, NOAA Satellite Aerosol Product Workshop, Sept. 25-26, 2017, College Park, MD, USA.

Hains, J. C., Chen,L.W. A., B. F. Taubman, B. G. Doddridge, R. R. Dickerson, 2007. A Side-by-Side comparison of Filter-Based PM2.5 Measurements at a Suburban Site: A Closure Study, Atmos. Environ., 41(29), 6167-6184.

Han, Y., Wu, Y., Wang. T., Zhuang, B., Li S., Zhao K., 2015. Impacts of elevated-aerosol-layer and aerosol type on the correlation of AOD and particulate matter with ground-based and satellite measurements in Nanjing, southeast China, Science of The Total Environment, 532, 195-207.

Hoff, R. M., Christopher, S. A., 2009. Remote sensing of Particulate Pollution from Space: Have we reached the Promised Land, J. Air Waste Manage. Assoc., **59**, 645–675.

Holben, B.N., T. F. Eck, I. Slutsker, D. Tanré, J.P. Buis, A. Setzer, E. Vermote, J.A. Reagan, Y.J. Kaufman, T. Nakajima, F. Lavenu, I. Jankowiak, A. Smirnov, 1998. AERONET - A federated instrument network and data archive for aerosol characterization, Rem. Sens. Environ., 66, 1-16.

Hogrefe, C., W. Hao, K. Civerolo, J. Ku, G. Sistla, R. Gaza, L. Sedefian, K. Schere, A. Gilliland, and R. Mathur, 2007. Daily Simulation of Ozone and Fine Particulates over New York State: Findings and Challenges. J. Appl. Meteor. Clim., **46**, 961–979, doi: 10.1175/JAM2520.1.

Huang, J., J. McQueen, J. Wilczak, I. Djalalova, I. Stajner, P. Shafran, D. Allured, P. Lee, L. Pan, D. Tong, H. Huang, G. DiMego, S. Upadhayay, L. Monache, 2017. Improving NOAA NAQFC $PM_{2.5}$ predictions with a bias correction approach, Wea. and Forecasting, 32, 407-421.

Janjie, Z. I., J. P. Gerrity Jr., and S. Nickovic, 2001. An alternative approach to nonhydrostatic modeling. Mon. Wea. Rev., 129, 1164–1178, doi: 10.1175/1520-0493.

Kalnay, E., M. Kanamitsu, R. Kistler, W. Collins, D. Deaven, L. Gandin, M. Iredell, S. Saha, G. White, J. Woollen, Y. Zhu, A. Leetmaa, R. Reynolds, M. Chelliah, W. Ebisuzaki, W. Higgins, J. Janowiak, K. C. Mo, C. Ropelewski, J. Wang, Roy Jenne, Dennis Joseph, 1996. The NCEP/NCAR reanalysis 40-year project, Bull. Amer. Meteor. Soc., 77, 437-471

Kelly, J. T., P. V. Bhave, C. G. Nolte, U. Shankar, K. M. Foley, 2009. Simulating emission and chemical evolution of coarse sea-salt particles in the Community Multiscale Air Quality (CMAQ) model. Geosci. Model Dev., 2, 1335–1374, doi:10.5194/gmdd-2-1335-2009.

Lee, P., J. McQueen, I. Stajner, J. Huang, L. Pan, D. Tong, H. Kim, Y. Tang, Kondragunta, M. Ruminski, S. Lu, E. Rogers, R. Saylor, P. Shafran, H. Huang, J. Gorline, S. Upadhayay, R. Artz, 2016. NAQFC developmental forecast guidance for fine particulate matter (PM2.5). Wea. and Forecasting. doi:10.1175/WAF-D-15-0163.1.

Li, S., Joseph E., Min, Q., 2016. Remote sensing of ground-level PM2.5 combining AOD and backscattering profile, Remote Sensing of Environment, 183, 120-128.

Liu, Y., Wang, Z., Wang, J., Ferrare, R. A., Newsom, R. K., Welton, E. J., 2011. The effect of aerosol vertical profiles on satellite-estimated surface particle sulfate concentrations, Remote Sensing of Environment, 115 (2), 508-513.

Liu, Y., Goodrick, S., Heilman, W., 2014. Wildland fire emissions, carbon, and climate: Wildfire–climate interactions. Forest Ecol. Manage., 317, 80–96.

Masiol, M., P. K. Hopke, H.D. Felton, B.P. Frank, O.V. Rattigan, M.J. Wurth, G.H. LaDuke, 2017. Analysis of major air pollutants and submicron particles in New York City and Long Island, Atmos. Environ., 148, 203-214.

Menut L, Flamant C, Pelon J, Flamant PH, 1999. Urban Boundary-Layer Height Determination from Lidar Measurements Over the Paris Area, Appl. Opt. 38: 945-954.

Miller, D. J., K. Sun, M. A. Zondlo, D. Kanter, O. Dubovik, E. J. Welton, D. M. Winker, P. Ginoux, 2011. Assessing boreal forest fire smoke aerosol impacts on U.S. air quality: A case study using multiple data sets, J. Geophys. Res., 116, D22209, doi:10.1029/2011JD016170.

Münkel, C., Räsänen, J., 2004. New optical concept for commercial lidar ceilometers scanning the boundary layer, Proc. SPIE, 5571, 364-374.

Omar, A. H., Winker, D. M., Kittaka, C. et al., 2009. The CALIPSO Automated Aerosol Classification and Lidar Ratio Selection Algorithm, J. Atmos. Oceanic Technol., 26 (10), 1994–2014.

O'Neill, S. M., and Coauthors, 2009. Regional real-time smoke prediction systems. Wildland Fires and Air Pollution, A. Bytnerowicz et al., Eds., Developments in Environmental Science, Vol. 8, Elsevier, 499–534.

Pachon, J. E., Weber, R. J., Zhang, X., Mulholland, J. A., Russell, G.A. 2013. Revising the use of potassium (K) in the source apportionment of $PM_{2.5}$, Atmos. Pollution Res., 4(1), 14-21.

Pahlow, M., Kleissl, J. & Parlange, M.B., 2005. Atmospheric boundary-layer structure observed during a haze event due to forest-fire smoke, Boundary-Layer Meteorol, 114 (1), 53-70.

Rattigan, Oliver V., H. D. Felton, M.S. Bae, J. J. Schwab, K. L. Demerjian, 2010. Multi-year hourly PM2.5 carbon measurements in New York: Diurnal, day of week and seasonal patterns, Atmos. Environ., 44 (16), 2043-2053.

Rattigan, Oliver V., K. L. Civerolo, H. D. Felton, J. J. Schwab, K. L. Demerjian, 2016. Long Term Trends in New York: $PM_{2.5}$ Mass and Particle Components, Aerosol and Air Quality Research, 16(5), 1191-1205.

Rees, S. L., Robinson, A. L, A. Khlystov, C. O. Stanier, S. N. Pandis, 2004. Mass balance closure and the Federal Reference Method for PM2.5 in Pittsburgh, Pennsylvania, Atmos. Environ., 38(20), 3305-3318.

Ruminski, M., S. Kondragunta, R. Draxler, J. Zeng, Recent Changes to the Hazard Mapping System, 2006. 15th International Emission Inventory Conference, Reinventing Inventories - New Ideas in New Orleans, New Orleans, May 15 – 18, 2016.

Russell, P.B., R. W. Bergstrom, Y. Shinozuka, A. D. Clarke, P. F. DeCarlo, J. L. Jimenez, J. M. Livingston, J. Redemann, O. Dubovik, and A. Strawa. 2010. Absorption Angstrom Exponent in AERONET and related data as an indicator of aerosol composition, Atmos. Chem. Phys., 10, 1155-1169.

Sapkota, A., Symons, J. M., Kleissl, J., Wang, L., Parlange, M. B., Ondov, J., Breysse, P. N., Diette, G. B., Eggleston, P. A., Buckley, T. J. 2005. Impact of the 2002 Canadian Forest Fires on Particulate Matter Air Quality in Baltimore City, *Environ. Sci. Technol.*, *39* (1), 24–32.

Schoennagel, T., J. K. Balch, H. Brenkert-Smith, P. E. Dennison, B. J. Harvey, M. A. Krawchuk, N. Mietkiewicz, P. Morgan, M. A. Moritz, R. Rasker, M. G. Turner, C. 2017. Whitlock, Adapt to more wildfire in western North American forests as climate changes, Proc. Natl. Acad. Sci., 114 (18), 4582-4590.

Sofowote, U., Dempsey,F., 2015. Impacts of forest fires on ambient near–real–time PM2.5 in Ontario, Canada: Meteorological analyses and source apportionment of the July 2011–2013 episodes, Atmos. Pollution Res., 6(1), 1-10.

Stull, Roland B., 1988. An Introduction to Boundary Layer Meteorology, Kluwer Academic Publishers.

Winker, D. M., M. A. Vaughan, A. Omar, Y. Hu, and K. A. Powell, Z. Liu W. H. Hunt, S. A. Young, 2009. Overview of the CALIPSO Mission and CALIOP Data Processing Algorithms, J. Atmos. Oceanic Technol., 26, 2310–2323.

Wu, Y., S. Chaw, B. Gross, F. Moshary, and S. Ahmed, 2009. Low and optically thin cloud measurements using a Raman-Mie lidar, Appl. Opt. 48, 1218-1227.

Wu, Y., L. Cordero, B. Gross, Moshary, F., Ahmed, S., 2012. Smoke plume optical properties and transport observed by a multi-wavelength lidar, sunphotometer and satellite, Atmos. Environ., 63, 32–42.

Wu, Y., Han Y., Voulgarakis, A., Wang, T., Li, M., Wang, Y., Xie, M., Zhuang, B., Li, S. (2017). An agricultural biomass-burning episode in eastern China: Transport, optical properties, and impacts on regional air quality, J. Geophys. Res. Atmos., 122, 2304–2324.

Zhang, X., S. Kondragunta, C. Schmidt, and F. Kogan, 2008. Near real time monitoring of biomass burning particulate emissions (PM2.5) across contiguous United States using multiple satellite instruments. Atmos. Environ., 42**,** 6959–6972.

Zhang, Y., M. Bocquet, V. Mallet, C. Seigneur, A. Baklanov, 2012. Real-time air quality forecasting, part II: State of the science, current research needs, and future prospects. Atmos. Environ. 60, 656-676.

Zhang, Y., Li, Z., 2015. Remote sensing of atmospheric fine particulate matter (PM2.5) mass concentration near the ground from satellite observation, Remote Sensing of Environment, 160, 252-262.

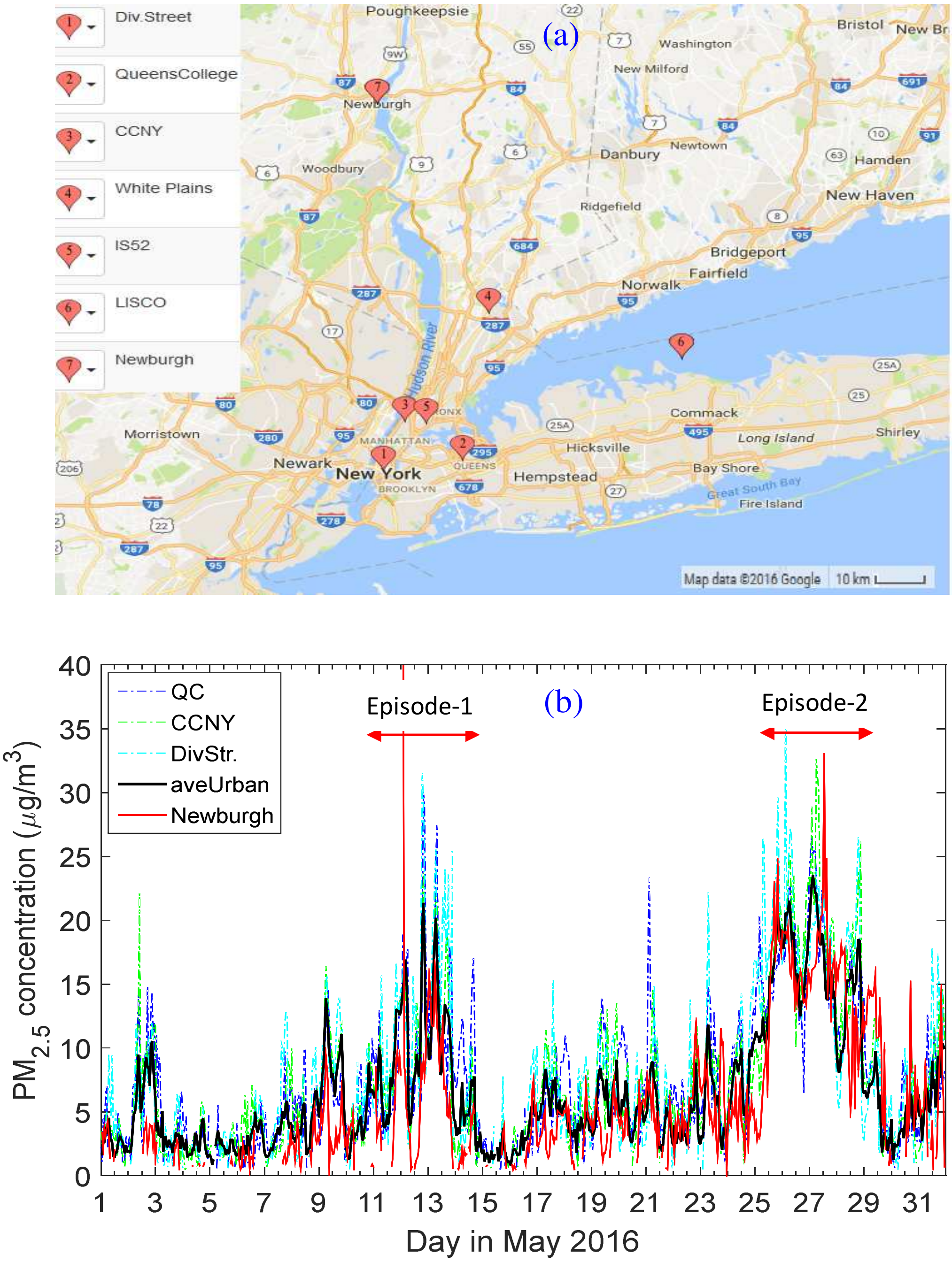

Fig. 1. (a) PM$_{2.5}$-site geolocations and (b) PM$_{2.5}$ concentration in NYC area, May 2016. Two episodes of PM$_{2.5}$ increase occurring on May 9-13 and May 25-29, respectively.

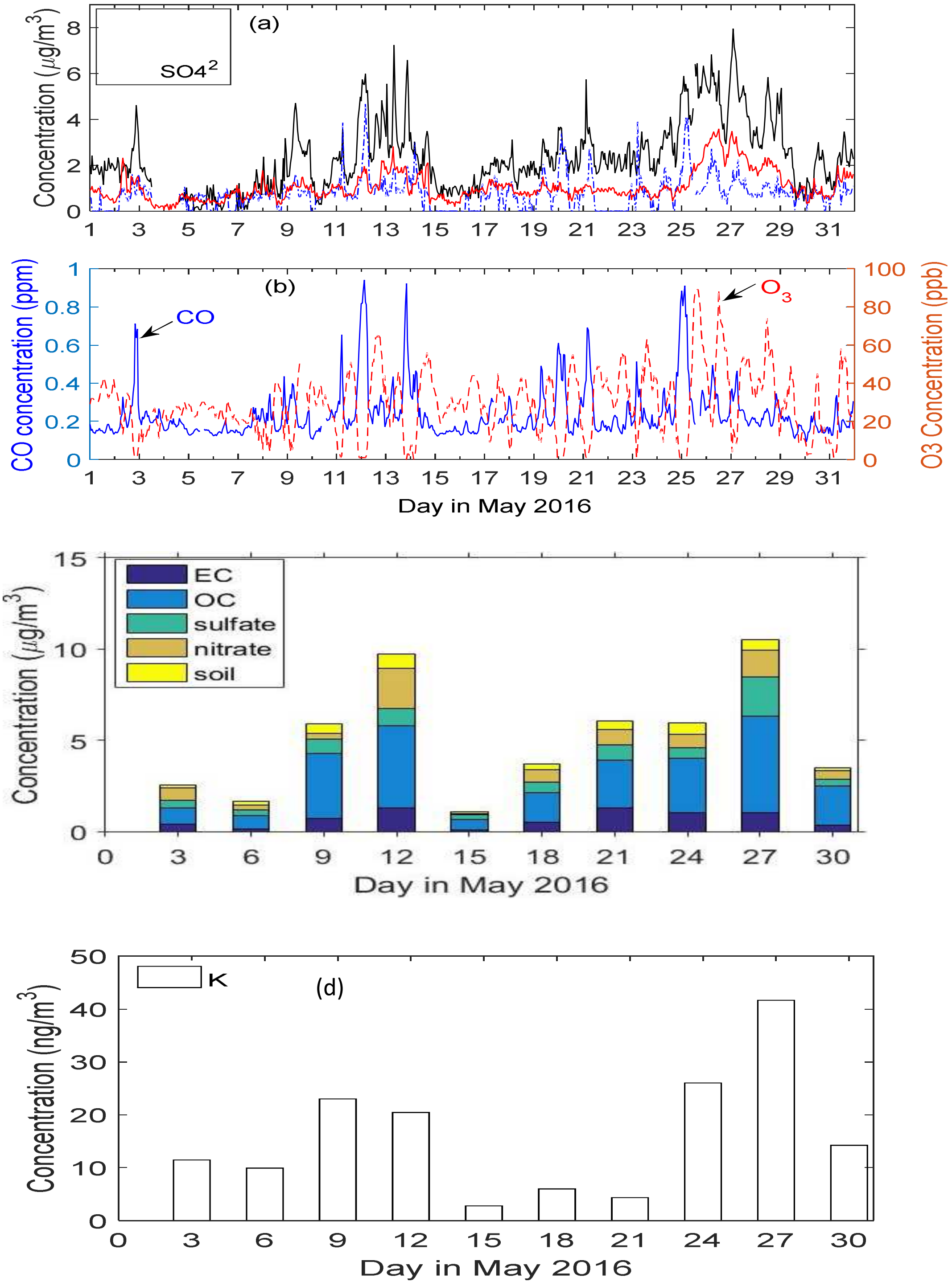

Fig. 2 Temporal variation of $PM_{2.5}$ speciation and ozone. (a) hourly average of OC, EC and sulfate, (b) ozone and CO, (c) daily average species (1-in-3), (d) Potassium ion (K^+) at QC site in May 2016.

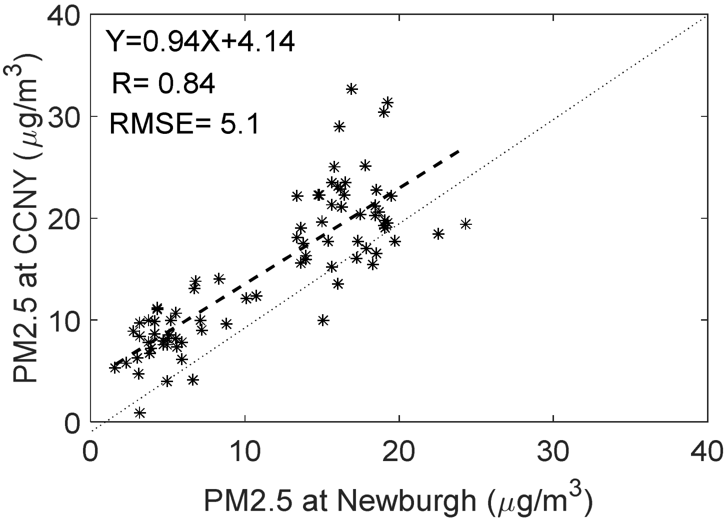

Fig.3 Correlation of $PM_{2.5}$ at CCNY (urban) and Newburgh (upwind rural) site.

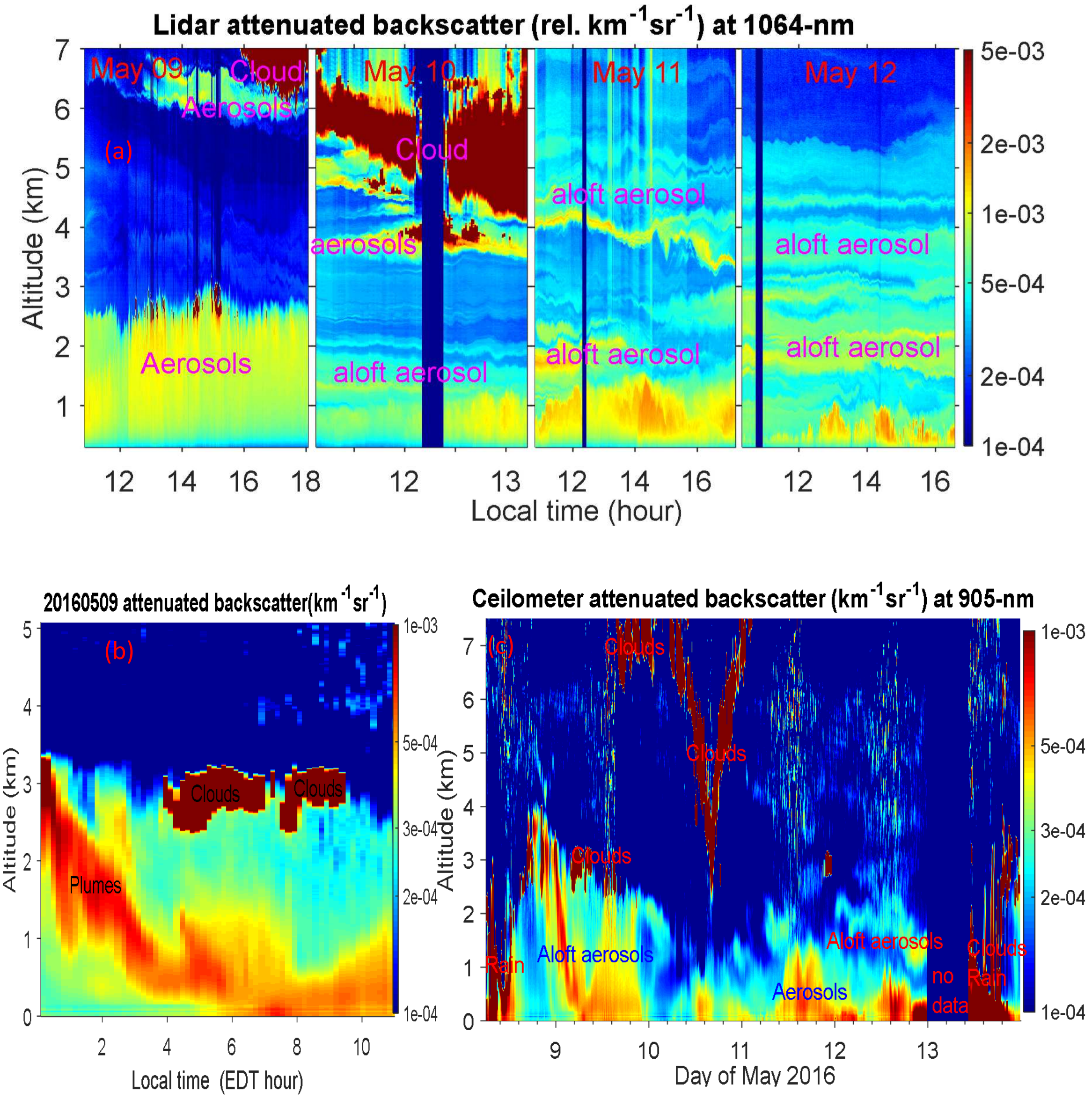

Fig. 4 (a) Range-resolved attenuated backscatter from CCNY-lidar during May 9-12, and (b)-(c) ceilometer images during May 8-13, 2016 (Episode I). Aloft plumes (yellow-red) and clouds (dark-red) can be seen.

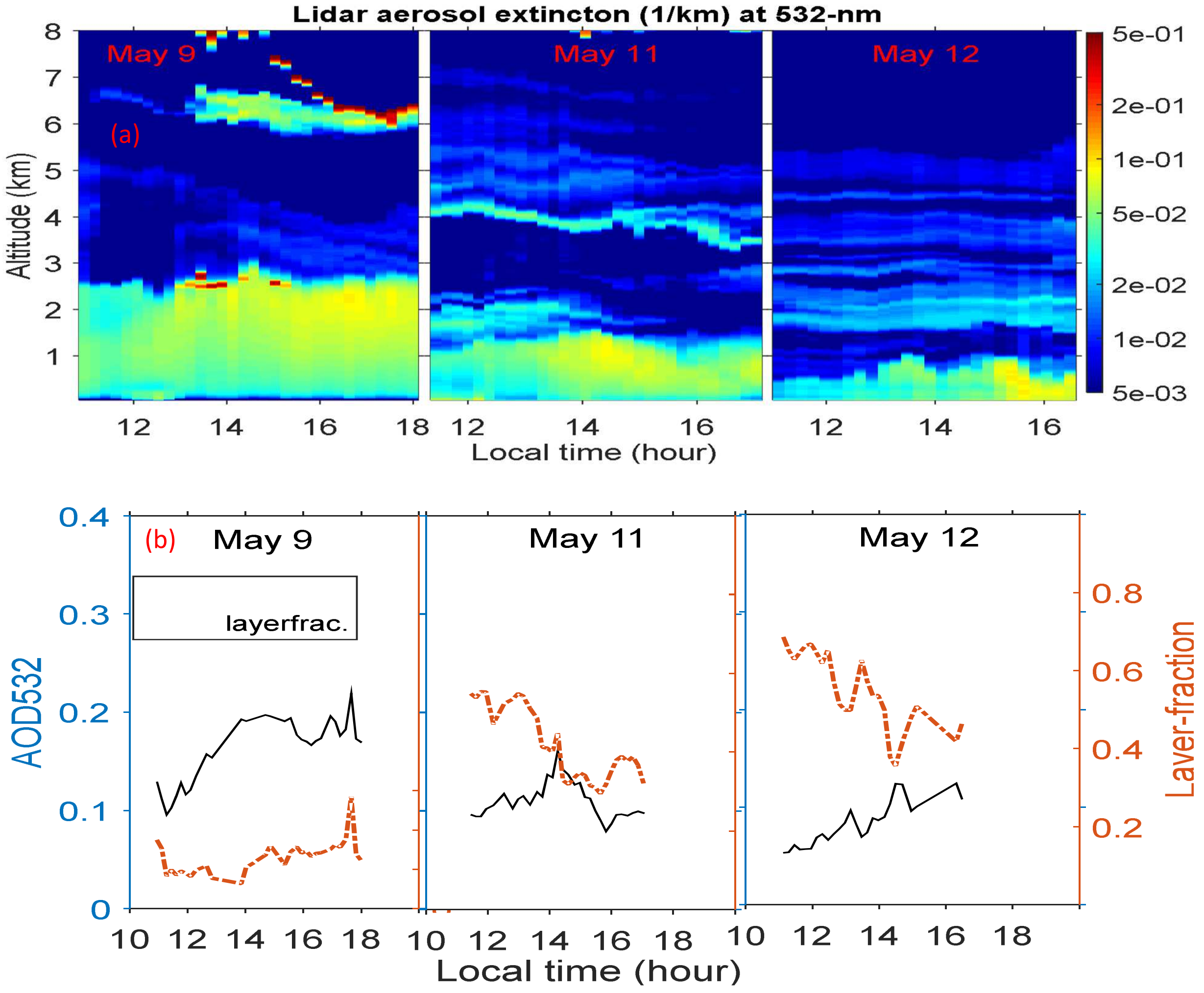

Fig. 5 (a) Aerosol extinction coefficients (10-min ave) at 532- nm, (b) total AOD and layer-AOD fraction from the CCNY-lidar during May 9-12, 2016.

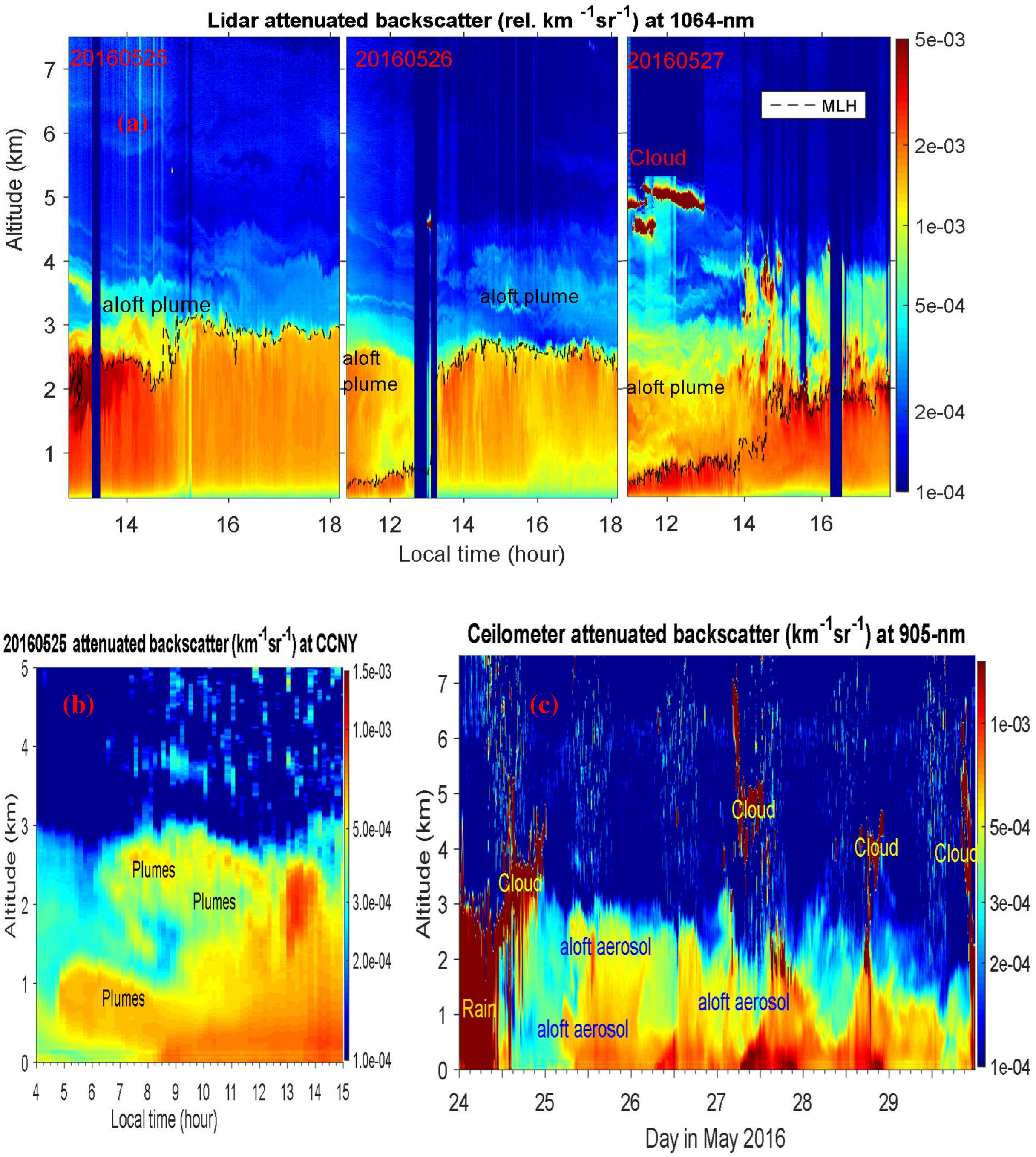

Fig. 6. (a) Range-resolved attenuated backscatter (dash line: MLH mixing-layer-height) from the CCNY-lidar on May 25-27 and (b)-(c) ceilometer data during May 24-29, 2016 (Episode II).

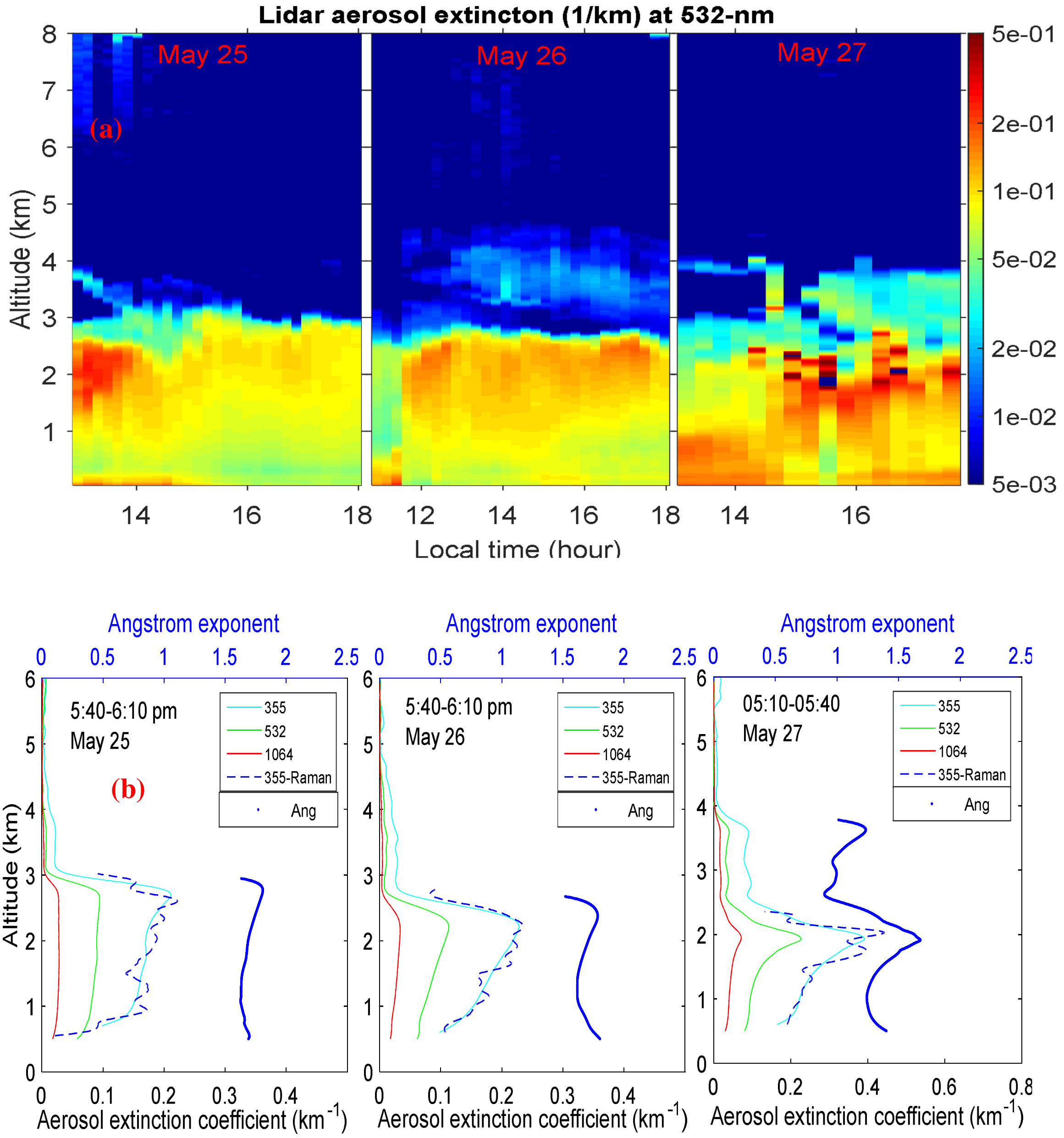

Fig. 7. (a) Aerosol extinction coefficient at 532-nm (10-min ave), (b) multi-wavelength extinction and Angstrom exponent profiles from CCNY-lidar on May 25-27, 2016

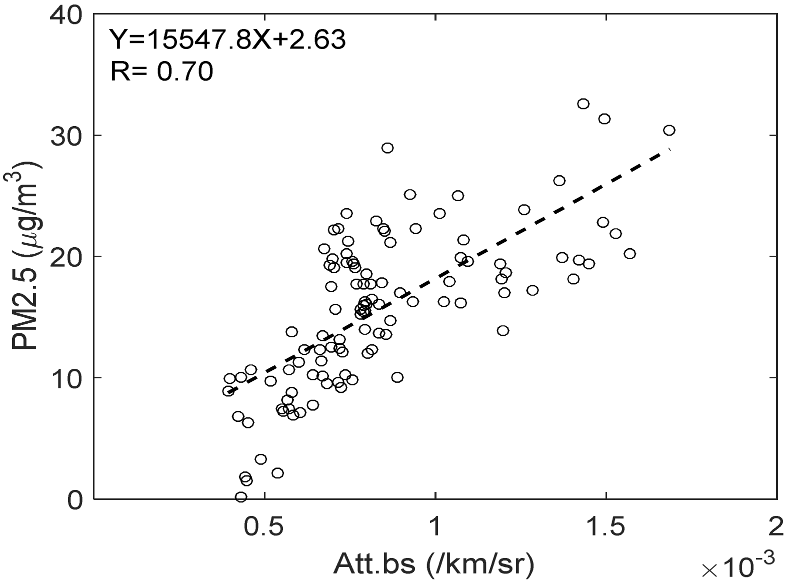

Fig. 8 Correlation of total attenuated backscatter and $PM_{2.5}$ at CCNY

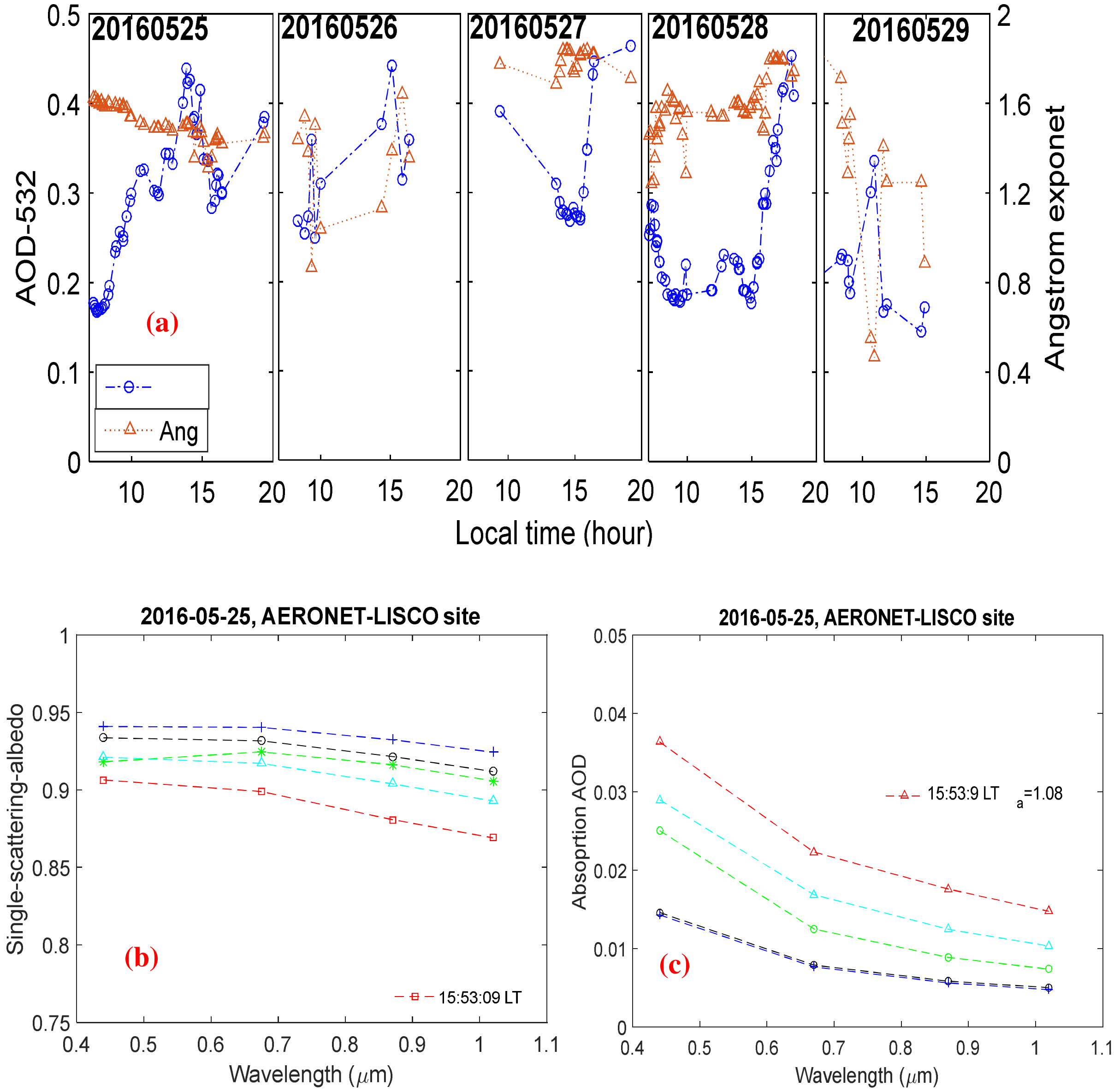

Fig. 9. Aerosol optical properties from the AERONET sunphotometer. (a) AOD and Angstrom exponent, (b) single-scattering-albedo, (c) absorbing AOD (a_α: Absorption Angstrom exponent).

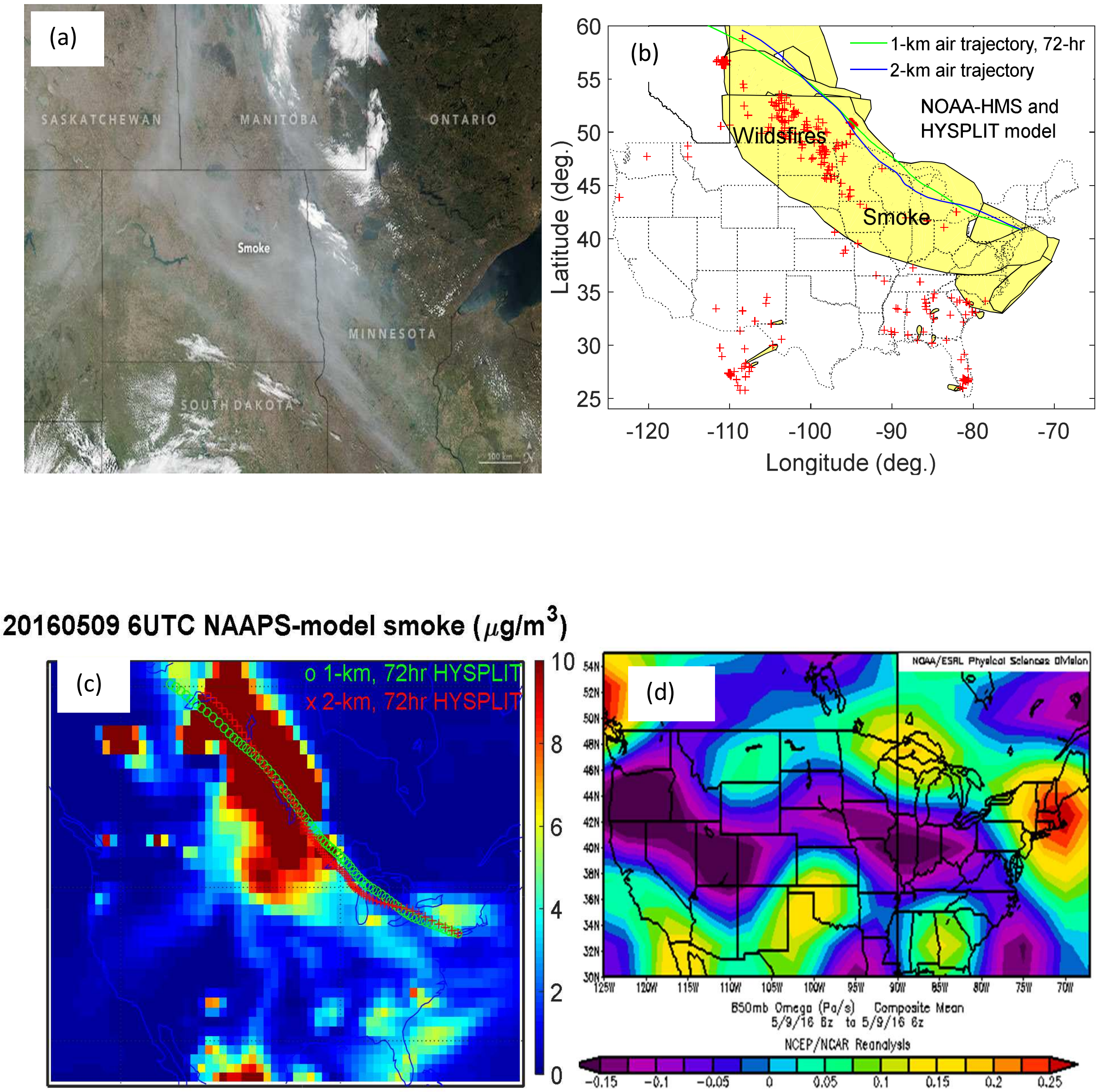

Fig.10 (a) MODIS image showing the smoke over the west Canada and northwest U.S, (b) Fire sources (red +), smoke areas (yellow) and backward trajectories (green and black lines) by NOAA-HMS and HYSPLIT model on May 9, 2016; (c) NAAPS model surface smoke at 6:00UTC on May 9, 2016; (d) NOAA/NCEP vertical wind speed at 850-mb level at 6:00 UTC on May 9, 2016 (a positive value corresponds to descending motion and a negative value corresponding to ascending motion)

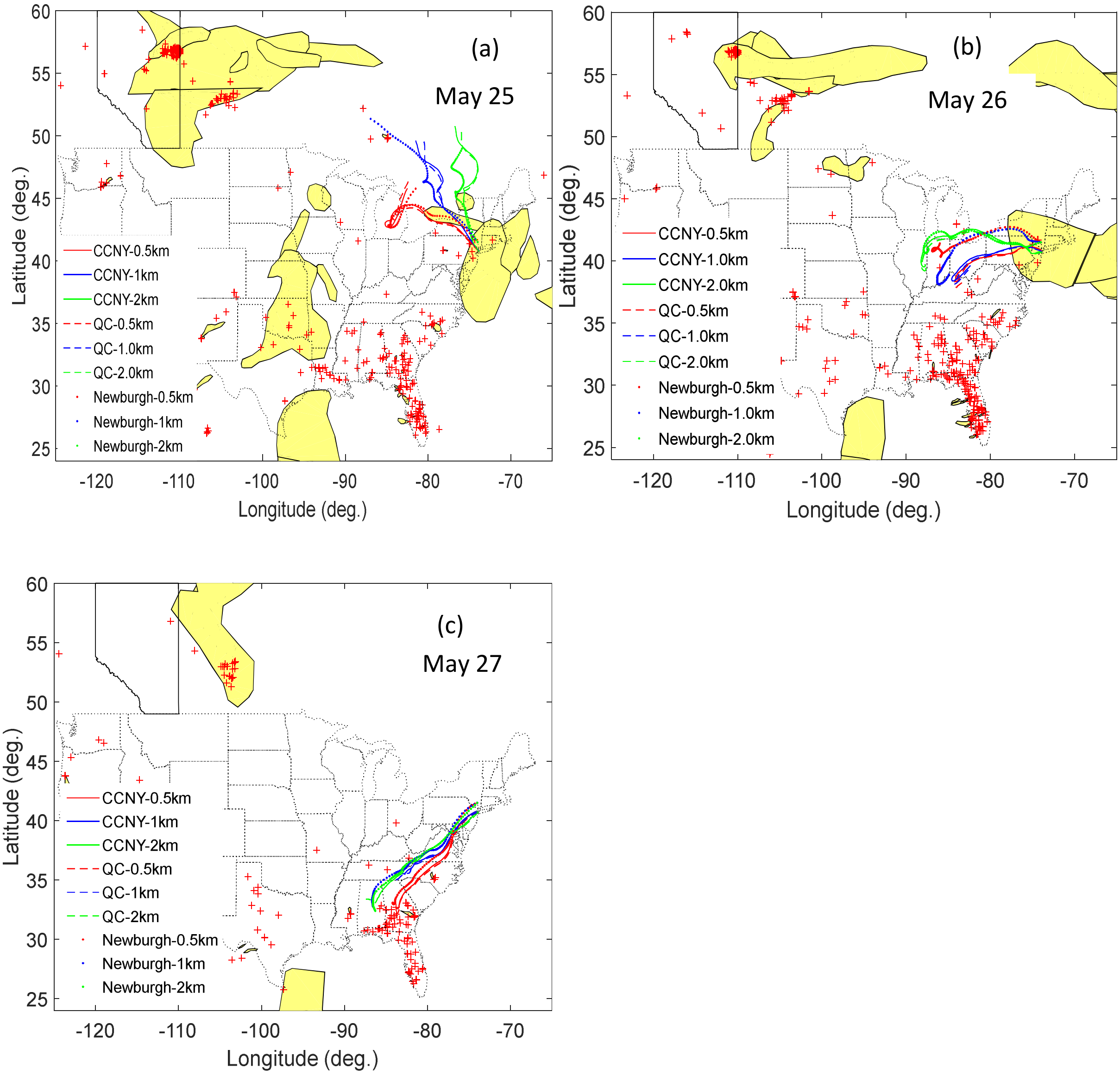

Fig.11 (a) -(c) Fire sources (red symbol +) and smoke areas (yellow) from the NOAA-HMS, and air backward trajectories (green-black lines) ending at three sites below 2-km altitude from the NOAA-HYSPLIT model ending at 12: 00 UTC on May 25 (transport from Canada), 26 (transport from the west US) and 27 (transport from the southeast US), respectively. Cloud cover hinders the fire/smoke detection from the satellites.

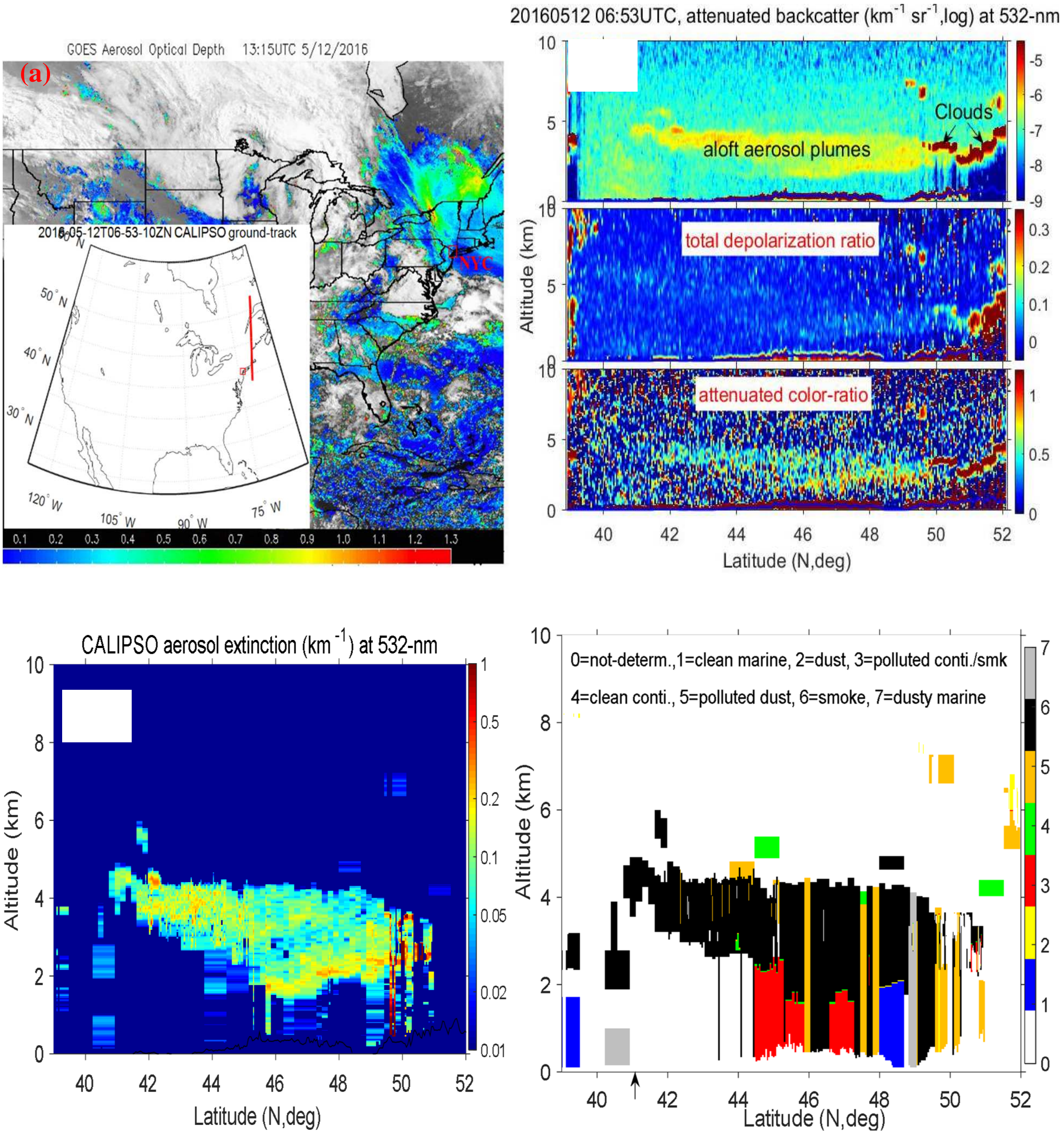

Fig. 12. (a) NOAA-GASP aerosol optical depth (AOD)(Color bar-AOD, high over in the north NYC; gray-cloud cover, a lot of clouds in north US and Canada) and CALIPSO ground track (red line) nearby the CCNY-site (red square), (b) attenuated backscatter, depolarization ratio and color ratio, (c) aerosol extinction and (d) aerosol subtypes (arrow in x-axis: nearest CCNY) on May 12, 2016.

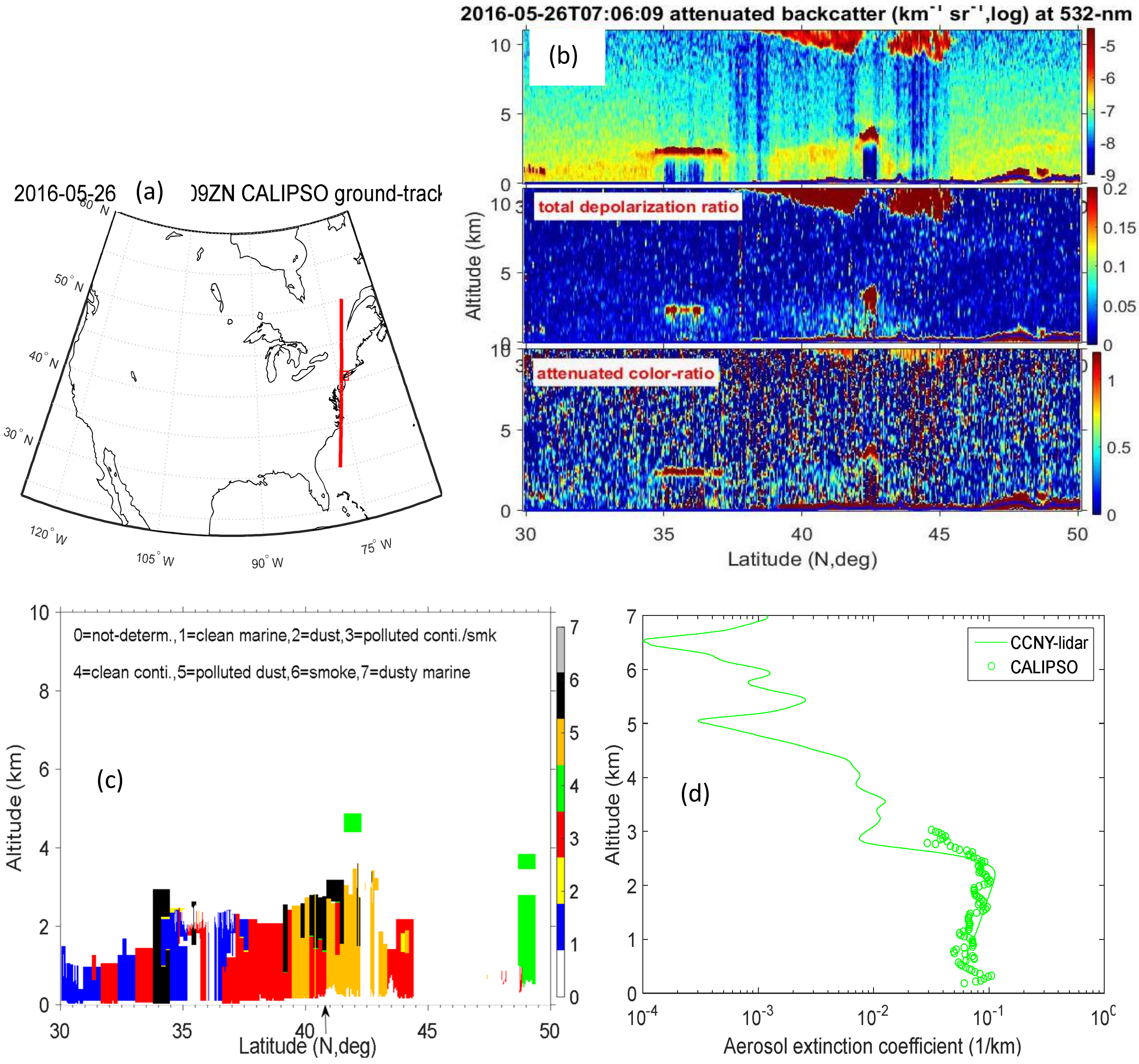

Fig. 13. (a) CALIPSO track (red line) nearby the CCNY site (red square), (b) attenuated backscatter, depolarization ratio, (c) aerosol subtypes (arrow in x-axis: nearest CCNY), and (d) aerosol extinction coefficient profiles nearby CCNY-lidar on May 26, 2016.

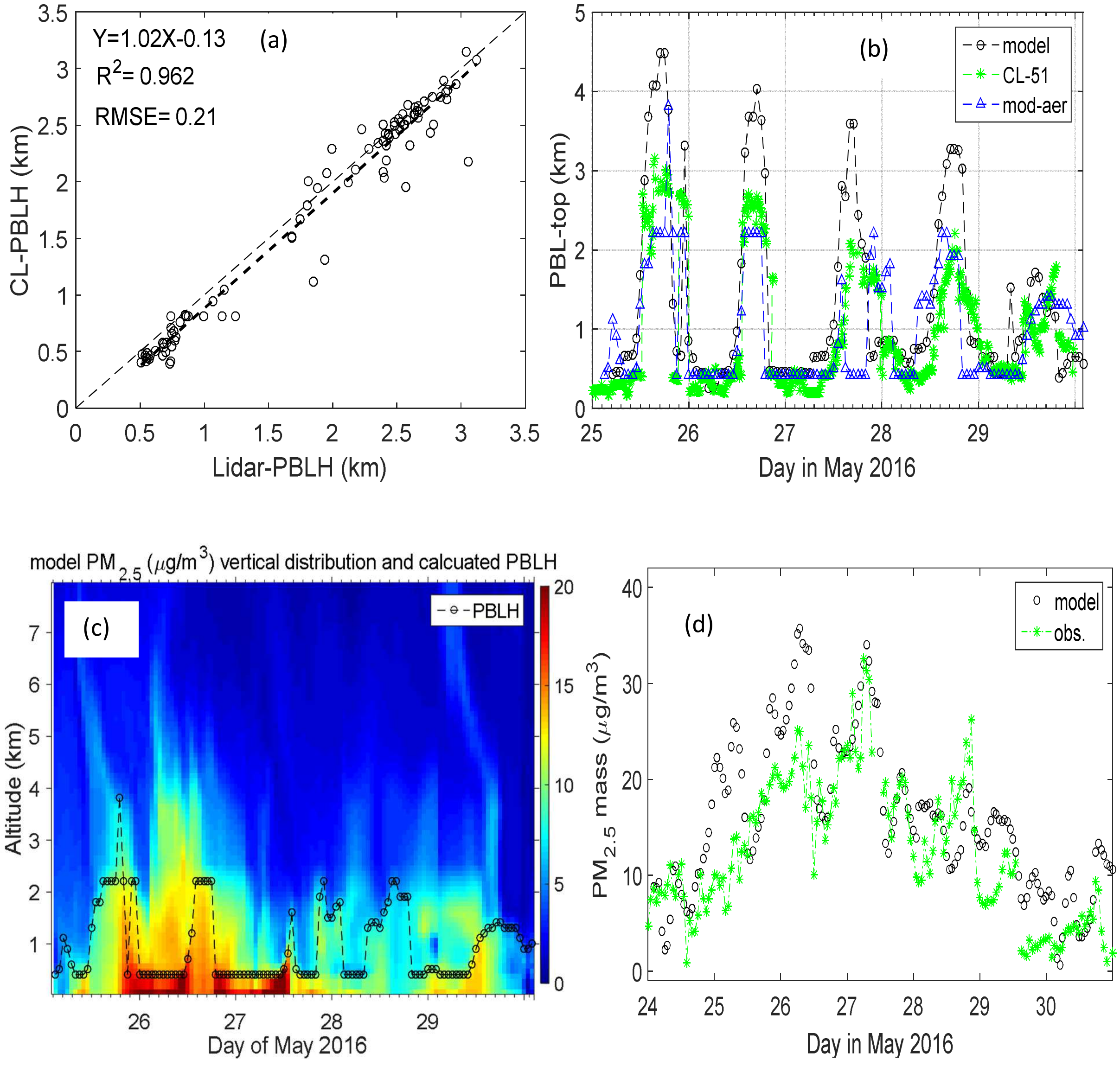

Fig. 14. Comparisons between the model and observations at CCNY site. (a) PBLH correlation between lidar and ceilometer, (b) PBL-top or PBLH from the model and observation, “model”: PBLH from the NAM meteorological-based value; “CL-51”: ceilometer-measurement; “mod-aer”: PBLH estimate from the model $PM_{2.5}$ profile; (c) $PM_{2.5}$ profiles from the model, and (d) $PM_{2.5}$ comparison between the model and ground observation.

Dense aloft smoke plume intrusion and mixing down into PBL are observed. A coincident increase of ground $PM_{2.5}$ in the NYC urban/rural area and the enhancement of OC, EC and K^+ indicate the big impacts of transported smoke on the local air quality.

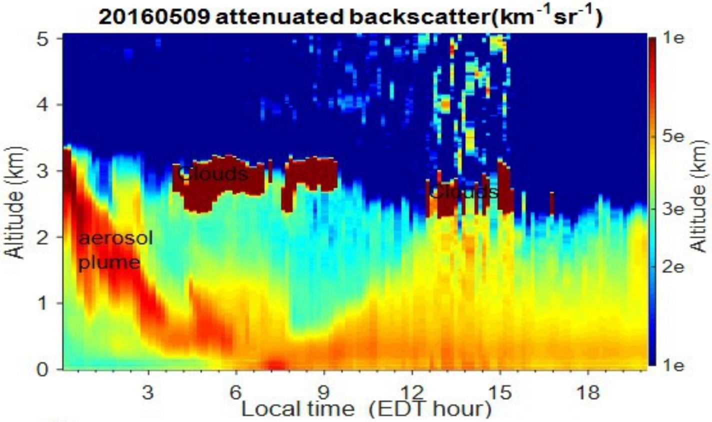
20160509 attenuated backscatter($km^{-1}sr^{-1}$)

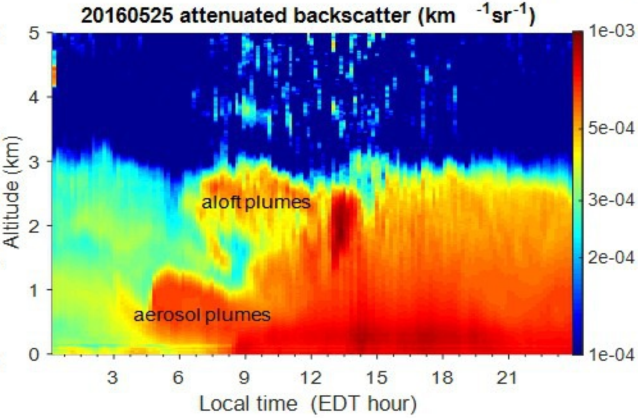
20160525 attenuated backscatter ($km^{-1}sr^{-1}$)